ISSN 2372-0352

AIMS Environmental Science

Volume No. 11
Issue No. 3
September - December 2024

ENRICHED PUBLICATIONS PVT.LTD

JE - 18,Gupta Colony, Khirki Extn,
Malviya Nagar, New Delhi - 110017.
E- Mail: info@enrichedpublication.com
Phone :- +91-8877340707

·ISSN 2372-0352

AIMS Environmental Science

Aims and Scope

AIMS Environmental Science is an international Open Access journal devoted to publishing peer-reviewed, high quality, original papers in the field of Environmental science. We publish the following article types: original research articles, reviews, editorials, letters, and conference reports.All published papers' full text from 2016 will be indexed by WoS.

Aim and scope

AIMS Environmental science is an international Open Access journal devoted to publishing peer-reviewed, high quality, original papers in the field of Environmental science. We publish the following article types: original research articles, reviews, editorials, letters, and conference reports.

AIMS Environmental science welcomes, but not limited to, the papers from the following topics:

- Global climate change & adaption
- Air-water-biota-rock interfaces
- Environmental epidemiology & ecology
- Pollution control & mitigation
- Environmental materials
- Natural resource management
- Waste management
- Geo-hazards
- Environmental risk analysis
- Air & water quality

·ISSN 2372-0352

AIMS Environmental Science

Editor in Chief

Yifeng Wang
Sandia National Laboratories, P.O. Box 5800, Mail Stop 0779,
Albuquerque, New Mexico 87185-0779

Managing Editor

Cheng Bi
Managing and Operation (Journal)

Editorial Board

Juan P. Arrebola	Laboratory of Medical Investigations, San Cecilio University Hospital, University of Granada, 18071-Granada, Spain
Giacomo Assandri	MUSE. Vertebrate Zoology Section Corso del Lavoro e della Scienza 3, I-38123, Trento, Italy
Imad A.M. Ahmed	The University of Lancaster, Lancaster Environment Centre, Lancaster, LA1 4YQ, United Kingdom
Angelo Albini	Dipartimento di Chimica Organica, Università di Pavia, via Taramelli 12, 27100 Pavia, Italy
Mohammednoor Altarawneh	Priority Research Centre for Energy, Faculty of Engineering & Built Environment, The University of Newcastle, Callaghan NSW 2308, Australia
Pasquale Avino	University of Molise, Campobasso, Italy
Alexander Baklanov	Science and Innovation Department, World Meteorological Organization (WMO) 7 bis, Avenue de la Paix, BP2300, CH-1211 Geneva 2, Switzerland
Georgios Bartzas	School of Mining and Metallurgical Engineering, National Technical University of Athens, Greece
Graham S. Begg	The James Hutton Institute, Invergowrie, Dundee DD2 5DA, UK
Cinzia Buratti	Department of Engineering, University of Perugia, Via G. Duranti 63, 06125 Perugia, Italy
Sivaraman (Siv) Balachandran	Department of Chemical and Environmental Engineering, University of Cincinnati, Cincinnati, OH 45221-0012, USA
Carlito B. Tabelin	Laboratory of Mineral Processing & Resources Recycling, Hokkaido University,Sapporo 001-0016, Japan
Andrew R. Barron	Department of Chemistry, Department of Materials Science, Rice University, Houston, Texas 77005, United States
Roberto Bono	Department of Public Health and Pediatrics, University of Torino, ITALY

Michel Boufadel	Department of Civil and Environmental Engineering, New Jersey Institute of Technology 323 MLK Blvd, Newark, NJ 07101 United States (610) 608-2281
Andrea Garcia Bravo	Department of Ecology and Genetics, Limnology, Uppsala University, Norbyvagen 18D, SE-75236 Uppsala, Sweden
Christopher R. Bryant	Geography, University of Montreal, Quebec, Canada and School of Environmental Design, University of Guelph, Ontario, Canada
Carlo Calfapietra	Institute of Agro-Environmental & Forest Biology (IBAF) - National Research Council (CNR),Via Marconi 2, 05010 Porano (TR), Italy
David Carvalho	The Centre for Environment and Marine Studies (CESAM), University of Aveiro, Portugal
Núria Castell	Norwegian Institute for Air Research, P.O. Box 100, NO-2027 Kjeller, Norway
Bing Chen	Northern Region Persistent Organic Pollution Control (NRPOP) Laboratory, Faculty of Engineering & Applied Science, Memorial University of Newfoundland, St. John's, NL A1B 3X5, Canada.
Renato Casagrandi	Dipartimento di Elettronica, Informazione e Bioingegneria (DEIB), Politecnico di Milano (PoliMI), Via Ponzio 34/5, 20133, Milano, Italia.
Hyeok Choi	Department of Civil Engineering, The University of Texas at Arlington, 437 Nedderman Hall, 416 Yates Street Arlington, TX 76019-0308, USA
WONG Man Sing, Charles	Department of Land Surveying and Geo-Informatics,The Hong Kong Polytechnic University
Ian Colbeck	School of Biological Sciences, University of Essex Wivenhoe Park, Colchester CO4 3SQ, UK
Federica Cucchiella	Department of Industrial and Information Engineering and Economics, University of L’Aquila, Via G. Gronchi 18, 67100, L’Aquila, Italy
Fatih Deniz	Department of Environmental Protection Technologies, Bozova Vocational School, Harran University, 63850 Bozova/Sanlýurfa, Turkey
Baolin Deng	Department of Civil and Environmental Engineering, University of Missouri, Columbia, Missouri 65211, USA
Steven D. Warren	USDA, US Forest Service Rocky Mountain Research Station Shrub Sciences Laboratory Provo, UT 84606-1856, USA
Sergi Díez	Department of Environmental Chemistry, Institute of Environmental Assessment and Water Research (IDAEA), Spanish National Research Council (CSIC), C/Jordi Girona, 18-26, E-08034 Barcelona, Spain
Florent Domine	UMI Takuvik, CNRS and Université Laval Pavillon Alexandre Vachon, Université Laval, Québec (Qc) G1V 0A6, Canada

Roy M. Harrison	Division of Environmental Health & Risk Management, School of Geography, Earth & Environmental Sciences, University of Birmingham, Edgbaston, Birmingham B15 2TT, UK
Norman Henderson	Prairie Adaptation Research Collaborative, University of Regina, Regina, Canada
Andrew Hoell	Department of Geography, University of California Santa Barbara, Santa Barbara, CA 93106 (805) 893-8000, USA
Robert W. Howarth	Department of Ecology & Evolutionary Biology, Corson Hall, Cornell University Ithaca, NY 14853 USA
Gordon Huang	Faculty of Engineering and Applied Science, University of Regina, Regina, Sask S4S 0A2, Canada
Nynke Hofstra	Environmental Systems Analysis Group, Wageningen University, P.O. Box 47, 6700 AA Wageningen, the Netherlands
Jeffrey Howard	Dept. of Geology, Wayne State University, 0224 Old Main Bldg. Detroit, MI 48202, USA
Pao Hsiao-Tien	Department of Management Science, National Yang Ming Chiao Tung University, Taiwan
Xiao-Lan Huang	Pegasus Technical Services Inc., 46 E. Hollister Street, Cincinnati, Ohio 45268, USA
Ellard Hunting	Department of Conservation Biology, Institute of Environmental Sciences (CML), Leiden University, Einsteinweg 2, NL-2333 CC, Leiden, The Netherlands
Carlo Ingrao	Department of Economics - University of Foggia; Via Romolo Caggese, 1 - 71121 Foggia, Italy
Ryan Jensen	Department of Geography, Brigham Young University, 622 Spencer W. Kimball Tower, Provo, UT 84602, USA
John Johnston	Ecosystems Research Division, National Exposure Research Laboratory, Office of Research and Development, U.S. Environmental Protection Agency, 960 College Station Road, Athens, Georgia 30605-2700, USA
Rebecca Jordan	Departments of Human Ecology & Ecology, Evolution, and Natural Resources, School of Environmental Biological Sciences, Cook Campus Rutgers, The State University of New Jersey, USA
Çetin KANTAR	Department of Environmental Engineering, Canakkale Onsekiz Mart University, Canakkale, Turkey
Helen M Karlsson	Department of Occupational and Environmental Medicine, Heart Medical Centre, County Council of Ostergotland, Linkoping University, 68185 Linkoping Sweden
Kasper Kok	Chairgroup Soil Geography and Landcape, Wageningen University & Research Droevendaalsesteeg 3a, 6708 PB Wageningen, the Netherlands

Arunprakash T. Karunanithi	Department of Civil Engineering|College of Engineering and Applied Science University of Colorado Denver, 1200 Larimer Street, NC 3027, Campus Box 113, P.O. Box 173364, Denver, CO 80217, USA
Anthony W. King	Environmental Sciences Division, Oak Ridge National Laboratory, P.O. Box 2008, Oak Ridge, TN 37831-6301, USA
Akio Koizumi	Department of Health and Environmental Sciences, Kyoto University Graduate School of Medicine, Kyoto, Japan
Prashant Kumar	Department of Civil and Environmental Engineering, University of Surrey, Guildford GU2 7XH, United Kingdom
He Liu	Department of Environmental Engineering, School of Environmental and Civil Engineering, Jiangnan University, Lihu Avenue 1800, Wuxi, Jiangsu Province, 214122, P. R.China
Yang Liu	Department of Civil and Environmental Engineering, University of Alberta, Edmonton, AB, T6G 2W2, Canada
Marc Levy	Center for International Earth Science Information Network (CIESIN), Earth Institute / Columbia University, 61 Route 9W Palisades, NY 10964, USA
Yuning Li	Department of Chemical Engineering, Department of Chemistry, and Waterloo Institute for Nanotechnology (WIN), University of Waterloo, QNC 5614, 200 University Ave West, Waterloo, Ontario, Canada
Stefano Loppi	Department of Life Sciences, University of Siena Via PA Mattioli 4, I-53100 Siena, Italy
Rafael Luque	Departamento de Química Orgánica, Universidad de Córdoba, Campus de Excelencia Agroalimentario CeiA3, Campus Universitario de Rabanales, Edificio Marie Curie (C3), E-14014 Córdoba, Spain
Piotr Matczak	Affliation: Institute of Sociology, Adam Mickiewicz University, Szamarzewskiego 89c 60-568 Poznan, Poland
Fabrizio Maturo	University of Campania Luigi Vanvitelli, Caserta, Italy
Paul T. Mativenga	Department of Mechanical, Aerospace & Civil Engineering, School of Engineering, The University of Manchester, Manchester, M13 9PL, United Kingdom
José Miguel Martínez-Paz	Department of Applied Economics., University of Murcia, Campus de Espinardo, 30100 Murcia, Spain
Cristina Menta	Department of Chemistry, Life Sciences and Environmental Sustainability,University of Parma
Justin P. Miller-Schulze	Department of Chemistry, California State University, Sacramento, 6000 J St. Sacramento, CA 95819, USA
Alexandra Monteiro	Department of Economy, Managemnet and Industrial Engineer, University of Aveiro, Aveiro, Portugal

Juan Moreno-Gutiérrez	Departamento de Máquinas y Motores Térmicos, Universidad de Cádiz, Campus Universitario Río San Pedro s/n, 11519 Puerto Real, Spain
Daniel Mueller	Department of Energy and Process Engineering, Norwegian University of Science and Technology, 7491 Trondheim, Norway
Mallikarjuna Nadagouda	US Environmental Protection Agency, National Risk Management Research Laboratory, 26 West Martin Luther King Drive, Cincinnati, OH 45268 USA
Cristina Nerín	Department of Analytical Chemistry, I3A, CPS-University of Zaragoza, María de Luna st. 3, Torres Quevedo Building, E-50018 Zaragoza, Spain
Chukwumerije Okereke	School of Human and Environmental Sciences, University of Reading, Po Box 233, RG6 6AB, UK
Bertram Ostendorf	Spatial Information Group, Earth and Environmental Sciences, University of Adelaide, Glen Osmond, SA 5064, Australia
Gang Pan	Department of Environmental Nanotechnology, Research Center for Eco-environmental Sciences, Chinese Academy of Sciences, 18 Shuangqing Road, Beijing 100085, China
Donguk Park	Department of Environmental Health, Korea National Open University
Alejandro J. Rescia Perazzo	Department of Biodiversity, Ecology and Evolution/Faculty of Biological Sciences, Complutense University of Madrid, Spain
Stefano Pierini	Dipartimento di Scienze e Tecnologie, Università di Napoli Parthenope, Centro Direzionale, Isola C4 - 80143 Napoli, Italy
Oleg S. Pokrovsky	Geoscience and Environment Toulouse, CNRS, Paris, France
Marcelo Francisco Pompelli	Plant Physiology Laboratory, Federal University of Pernambuco, Department of Botany, CCB, Recife, Pernambuco 50670901, Brazil
Albert A Presto	Department of Mechanical Engineering and Center for Atmospheric Particle Studies, Carnegie Mellon University, Pittsburgh, PA 15213, USA
Seeram Ramakrishna	Department of Mechanical Engineering, National University of Singapore, Singapore 117574, Republic of Singapore
Bernhard Rappenglueck	Department of Earth and Atmospheric Sciences (EAS), University of Houston, USA
Jingzheng Ren	The Hong Kong Polytechnic University, Hong Kong SAR, China University of Southern Denmark (Odense, Denmark) Institute for Security & Development Policy (Stockholm, Sweden)
Claire Richard	Equipe Photochimie, Clermont Université, Université Blaise Pascal, Institut de Chimie de Clermont-Ferrand (ICCF), BP

Marja-Liisa Riekkola	Department of Chemistry, University of Helsinki, Finland
Martin Leopold Romantschuk	Department Environmental Sciences, University of Helsinki, Niemenkatu 73, 15140 Lahti, Finland
David Rojas Rueda	Centre for Research in Environmental Epidemiology (CREAL), Parc de Recerca Biomèdica de Barcelona – PRBB, C. Doctor Aiguader, 88, 08003 Barcelona , Spain
Seena Sahadevan	Marine and Environmental Sciences Centre,,Dept. Life Sciences Faculty of Science and Technology, University of Coimbra P.O. box 3046, 3001-401 Coimbra, Portugal
Dimosthenis Sarigiannis	Department of Chemical Engineering, Aristotle University of Thessaloniki, Greece
Ajit Sarmah	Department of Civil & Environmental Engineering Faculty of Engineering, The University of Auckland, Private Bag 92019, Auckland, New Zealand
Biswajit Sarkar	Department of Industrial Engineering, Yonsei University, South Korea
Marta Schuhmacher	Environmental Engineering Laboratory, Departament d'Enginyeria Quimica, Universitat Rovira i Virgili, Av. Paisos Catalans 26, 43007 Tarragona, Catalonia, Spain
Laura Scrano	Department of European Cultures and Mediterranean (DICEM). University of Basilicata, Potenza – Italy
Jhy-Charm Soo	Health Effects Laboratory Division, National Institute for Occupational Safety and Health (NIOSH), Centers for Disease Control and Prevention, U.S. Department of Health and Human Services (DHHS)
Youngwoo Seo	Department of Civil Engineering, Department of Chemical and Environmental Engineering, University of Toledo, Toledo, Ohio, United States
Jesús Simal-Gándara	Nutrition and Bromatology Group, Analytical and Food Chemistry Department, Faculty of Food Science and Technology, University of Vigo, Ourense Campus, E32004 Ourense, Spain
Carla Patrícia Silva	Department of Chemistry and CESAM, University of Aveiro, Portugal
Karolina M. Siskova	Department of Physical Chemistry, Centre of Advanced Technologies and Materials (RCPTM), Palacky University, Olomouc, CR
Benjamin Sleeter	U.S. Geological Survey - Western Geographic Science Center, 345 Middlefield Road, Menlo Park, CA 94025, USA
Scott Smith	Department of Chemistry Wilfrid Laurier University, 75 University Avenue West, Waterloo, ON, N2L 3C5, CANADA
Christian Sonne	Department of Bioscience, Arctic Research Centre, Aarhus University, Frederiksborgvej 399 P.O. Box 358, DK-4000 Roskilde, Denmark

Sofia Sousa	LEPABE – Laboratory for Process Engineering, Environment, Biotechnology and Energy Chemical Engineering Department Faculty of Engineering, University of Porto, Rua Dr. Roberto Frias s/n, 4200-465 Porto, Portugal
Paul Sutton	Department of Geography and the Environment, 2050 East Iliff Ave, University of Denver, Denver, Colorado 80208, USA
Miklas Scholz	Division of Water Resources Engineering (TVRL), Department of Building and Environmental Technology, Faculty of Engineering, Lund University, P.O. Box 118, 22100 Lund, Sweden
Francesca Ugolini	8, Giovanni Caproni, 50145 Firenze, Italy
Nick Voulvoulis	Centre for Environmental Policy, Imperial College London, London SW7 2AZ, UK
Brigitte Tenhumberg	School of Biological Sciences (SBS) and Department of Mathematics, University of Nebraska-Lincoln (UNL), 412 Manter Hall, Lincoln, NE 68588-0118, USA
Ying I. Tsai	Department of Environmental Engineering and Science, Indoor Air Quality Research and Service Center, Chia Nan University of Pharmacy and Science, 60, Sec. 1, Erren Road, Rende District, Tainan City 71710, Taiwan
Mary Thornbush	Brock University, 500 Glenridge Avenue, St. Catharines, Ontario, L2S 3A1, Canada
Kai Wang	Department of Marine, Earth, and Atmospheric Sciences, North Carolina State University, Campus Box 8208, Raleigh, NC 27695, USA
Shaobin Wang	Department of Chemical Engineering and CRC for Contamination Assessment and Remediation of the Environment (CRC CARE), Curtin University, GPO Box U1987, Perth, WA 6845, Australia
Taoyuan Wei	Center for International Climate and Environmental Research – Oslo (CICERO), P.O. Box 1129 Blindern N-0318 Oslo, Norway
Dominik J Weiss	Department of Earth Science and Engineering, Imperial College London, South Kensington Campus, London SW7 2AZ, UK
J. Michael Wright	U.S. Environmental Protection Agency, National Center for Environmental Assessment, 26 W. Martin Luther King Drive (MS-A110), Cincinnati, OH 45268, USA
Fengchang Wu	State Key Laboratory of Environmental Criteria and Risk Assessment, State Environmental Protection Key Laboratory of Lake Pollution Control, Chinese Research Academy of Environmental Sciences, Beijing 100012, China

·ISSN 2372-0352

AIMS Environmental Science

(Volume No. 11 Issue No. 3, Sep - Dec 2024)

Contents

Addition of chitosan to calcium-alginate membranes for seawater NaCl adsorption

Anugrah Ricky Wijaya*, Alif Alfarisyi Syah, Dhea Chelsea Hana and Helwani Fuadi Sujoko Putra
Department of Chemistry, Faculty of Mathematics and Natural Sciences, Universitas Negeri Malang, Jl. Semarang 5 Malang 65145, Indonesia

ABSTRACT

Initial research was focused on the production of calcium-based alginate-chitosan membranes from coral skeletons collected from the Gulf of Prigi. The coral skeleton's composition was analyzed using XRF, revealing a calcium oxide content ranging from 90.86% to 93.41%. These membranes showed the significant potential for salt adsorption, as evidenced by FTIR analysis, which showed the presence of functional groups such as -OH, C=O, C-O, and N-H involved in the binding process. SEM analysis showed the particle size diameter of 185.96 nm, indicating a relatively rough and porous morphology. Under optimized conditions, the resulting calcium-based alginatechitosan membrane achieved 40.5% Na+ and 48.39% Cl- adsorptions, using 13.3 mL of 2% (w/v) chitosan and 26.6 mL of 2% (w/v) alginate with a 40-minutes contact time. The subsequent we applied for the desalination potential of calcium alginate, revealing the efficient reduction of NaCl levels in seawater. The calcium of coral skeletons collected was 90.86% and 93.41% before and after calcination, respectively, affirming the dominant calcium composition suitable for calcium alginate production. We identified an optimal 8-minute contact time for calcium alginate to effectively absorb NaCl, resulting in an 88.17% and 50% for Na+ and Cl- absorptions. We applied the addition of chitosan into calciumalginate membranes and its impact on enhancing salt adsorption efficiency for seawater desalination.

Keywords: Ca-alginate; chitosan; adsorption; Cl-; Na+

1. Introduction

The coastal regions often face water scarcity despite the proximity to abundant seawater resources due to challenges in obtaining clean water [1]. Seawater, with an average salinity of 3.5% and a salinity measurement of around 35 psu, contains NaCl rendering and unsuitable for direct human consumption [2]. The salinity measurement and Total Dissolved Solids (TDS) ranging from 20.000 to 50.000 ppm in the Gulf of Prigi is needed for desalination processes [3–5]. Desalination offers a viable solution, often utilizing adsorption methods involving membrane technology, which efficiently reduce NaCl levels in seawater [6]. The demand for clean water remains a challenge, necessitating innovative solutions.

The exploration of calcium-based membranes for salt adsorption was aimed to optimize desalination efficiency [7]. The membranes synthesized from coral skeletons, predominantly composed of calcium carbonate (CaCO3), are augmented with chitosan and sodium alginate, providing a cost-effective yet efficient solution for desalination [8,9]. The membrane synthesis process involves the crosslinking of sodium alginate and calcium, forming calcium alginate membranes capable of adsorbing NaCl from seawater [10,11].

Chitosan, a biopolymer with active NH2 and OH- functional groups, holds potential for membrane manufacturing, specifically in adsorption applications [12]. Combination chitosan with alginate potentially enhances the membrane's properties, potentially forming pores and binding with metals [13,14]. The coral skeleton is a significant resource for calcium-based membrane production [9]. The extraction of calcium oxide (CaO) from coral skeletons through the calcination process further improves the membrane's functional properties [15]. Through future desalination, power material membranes aim to transform mineral-rich seawater into clean water in coastal areas where water supply remains insufficient [16].

Here, the synthesis of calcium alginate membranes involve the utilization of abundant coral skeletons, primarily composed of CaCO3, and crosslinked with sodium alginate and calcium to form membranes capable of binding salt from seawater [17,18]. The combined coral skeletons and polymer materials like chitosan and sodium alginate in membrane synthesis provided a significant step toward creating efficient and cost-effective desalination methods [19]. We explored the addition of chitosan to calcium-alginate membranes for enhanced seawater salt adsorption, further advancing the development of viable desalination processes.

2. Experimental detail

2.1. Materials

The materials were coral skeletons, chitosan powder, sodium alginate, 37% HCl solution, NaCl solid, 1% K2CrO4 solution, AgNO3 solid, distilled water, NaOH solution, and filter paper.

2.2. Methods

2.2.1. Sample coral preparation

Corals taken from Prigi Beach undergo a series of preparation stages, such as cleaning with demineralized water, drying at 60 °C until dryness, grinding and sieving (200 mesh) until a fine powder was obtained. The resulting coral powder was calcined at 800 °C for 2 hours to produce high purity CaCO3 [20,21].

2.2.2. Preparation of CaCl2 solution from calcined coral

This CaCO3 was processed into a homogeneous CaCl2 solution, starting with diluting 83.3 mL of 37% HCl to obtain a 1 M HCl solution. Five grams of CaCO3 was combined with 100 mL of 1 M Hcl solution, producing a CaCl2 solution after homogenization and filtration.

2.2.3. Preparation of alginate and chitosan solutions

A total of 1 and 2 g of sodium alginate were individually weighed and each added to 100 mL of distilled water. The solutions were stirred using a hotplate magnetic stirrer at 300 rpm at 80 °C and left for 24 hours. Chitosan was prepared in concentrations of 1%, 2%, and 3%, respectively. A total of 1, 2, and 3 g of chitosan powder (w/v) were added to 100 mL of acetic acid solution with a concentration corresponding to the chitosan mass (1%, 2%, and 3% acetic acid). The solutions were then stirred using a hotplate magnetic stirrer at 300 rpm at 80 °C and left for 24 hours.

2.2.4. Synthesis of calcium- alginate-chitosan membranes

The synthesis of Ca-alginate-chitosan membranes was carried out by mixing the polymer solutions (sodium alginate and chitosan) in a volume of 40 mL with a chitosan-to-alginate ratio of 1:2, resulting in a chitosan solution volume of 16.13 mL and a sodium alginate solution volume of 26.6 mL with the variation concentration ratio of chitosan to alginate (1:1, 1:2, 1:3, 1:4). After 24 hours, the alginate-chitosan mixture was added with 10 mL of 0.5 M CaCl2 and left for 8 hours, followed by lifting and drying at room temperature for 24 hours. The resulting beads and transparent membranes were then characterized by measuring pH and washing with distilled water.

2.2.5. Optimization of calcium- alginate-chitosan membrane synthesis

The process of optimizing the concentration of the alginate solution involved adsorption experiments with NaCl solutions using different chitosan-alginate compositions. This aims to determine the optimum alginate composition that produces the highest Cl- adsorption concentration. Further optimization was focused on determining the ideal chitosan concentration for maximum Cl- adsorption. The characterized membranes were applied by FT-IR analysis to identify functional groups and SEM analysis for microstructural observation.

2.2.6. Characterization of calcium- alginate-chitosan membrane synthesis

The initial characterization of Calcium- Alginate-Chitosan Membrane Synthesis involved employing a Fourier transform infrared spectrometer (FT-IR, Shimadzu IR Prestige 21) to identify the compounds' functional groups. Subsequently, X-ray fluorescence (PANalytical) determined the elemental composition of a material/sample, while Scanning Electron Microscopy and Energy Dispersive X-ray (SEM EDX) can be used to characterize a material and its morphology.

2.2.7. Adsorption experiments

In laboratory scale applications, the membrane was tested by stirring a 0.1 N NaCl solution with varying contact times. The resulting solution underwent Na+ concentration analysis using AAS (Thermo scientific ICE3000) after appropriate dilution. In addition, analysis of Cl- concentration was carried out via Mohr's argentometric titration, which involves titration with a 0.1 N AgNO3 standard solution.

After adsorption, the filtrate was analyzed for Na+ and Cl- concentrations using specific techniques. The Na+ concentration was determined using AAS after adequate dilution, while the Cl- concentration was determined via Mohr's argentometry titration involving titration with a 0.1 N AgNO3 standard solution, both carried out in duplicate for accuracy. Blank titration was carried out as a reference for calculating Cl- levels.

3. Results and discussion

3.1. Characterization of coral skeleton using XRF Test

The sieved coral skeleton was calcined at 800 °C to obtain high purity calcium oxide. Calcination functions remove CO2, dirt, and minerals other than calcium. During this process, heat was applied to the surface of the coral particles, thereby encouraging the released CO2 gas to migrate to the surface and disperse into the calcined sample. The resulting calcined coral as the natural sources for material CaCl2 productions. XRF analysis of corals determines the content of calcium and various other elements. The elemental composition of coral, both before and after calcination is listed in Tables 1 and 2.

Table 1. XRF Analyses of coral before alcination.

No	Elements	Wt (%)	Oxide	Wt (%)
1	Ca	90.82	CaO	90.86
2	Si	1.30	SiO_2	2.30
3	Sr	4.40	SrO	3.42
4	Fe	1.70	Fe_2O_3	1.62
5	Ti	0.15	TiO_2	0.16
6	Mo	0.89	MoO_3	1.10
7	Cu	0.03	CuO	0.03
8	Mn	0.07	MnO	0.06
9	Ba	0.10	BaO	0.10
10	Yb	0.47	Yb_2O_3	0.35
11	Lu	0.09	Lu_2O_3	0.06

Table 2. XRF analyses of coral after calcination.

No	Elements	Wt (%)	Oxide	Wt (%)
1	Ca	92.58	CaO	93.41
2	Si	-	SiO_2	-
3	Sr	4.54	SrO	3.56
4	Fe	-	Fe_2O_3	1.43
5	Ti	0.11	TiO_2	0.12
6	Mo	1.10	MoO_3	1.30
7	Cu	0.04	CuO	0.03
8	Mn	0.06	MnO	0.05
9	Ba	0.10	BaO	0.08
10	Yb	-	Yb_2O_3	-
11	Lu	-	Lu_2O_3	-

The XRF measurements showed that the coral was composed mainly of calcium oxide, which has the potential to be used as a component of Ca2+ in the membrane. The percentage of CaO before and after calcination was 90.82 and 93.41%, respectively.

3.2. Synthesis of calcium-alginate-chitosan

The process of dissolving sodium alginate in water using a hotplate magnetic stirrer is recommended at 80 °C with a speed of 300 rpm [22]. Chitosan powder was dissolved in highconcentration acetate acid or organic acid solvents with a pH range of 4–6 [22]. Furthermore, chitosan was dissolved at a relatively high temperature, around 80°–100°C. The solubility process of chitosan occurs through a protonation reaction, where the amine group (-NH2) in chitosan accepts H+ released by acetic acid, resulting in a positive charge (-Nh3+). The addition of Ca2+ ion from CaCl2 reacted as a cross-link with sodium alginate and chitosan. CaCl2 functions as a crosslinking bound sodium alginate, with Ca2+ replacing Na+ to form calcium alginate. That cross link is essential for the formation of the gel structure. The formation of Ca-alginate-chitosan involves a drip technique, where a vacuum pump ensures a consistent drip frequency of the sodium alginate solution into the calcium chloride solution.

During Ca-alginate-chitosan beads production, the NaCl was removed through washing, achieved by soaking the beads in distilled water. The process requires a 300 mL sodium alginate solution and 150 mL of calcium chloride solution to release 100 grams of calcium alginate granules. This method is widely used in various scientific studies and industrial applications, and offers a controlled and efficient means of producing calcium alginate beads for diverse uses.

Figure 1. Ca-alginate-chitosan beads.

3.3. Characterization of Calcium-Based Alginate-Chitosan Membrane Using FTIR

The calcium alginate-chitosan membrane was analyzed using FTIR to determine the functional group content present in the membrane. FTIR spectrum analysis was performed using the Origin application. The FTIR characterization is shown in Figure 2.

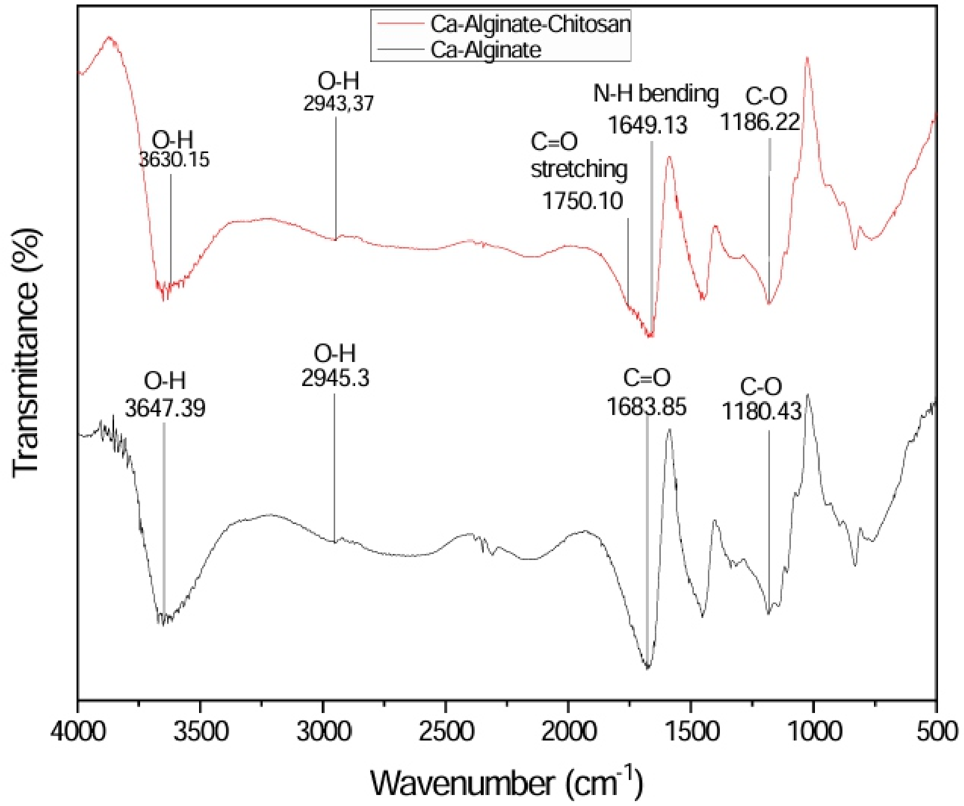

Figure 2. FTIR Spectra of Calcium Alginate Membrane and Calcium Alginate-Chitosan Membrane.

The infrared (IR) spectrum shows characteristic features of calcium alginate and calcium alginatechitosan membranes. In the calcium alginate spectrum, the prominent peak at 1683.85 cm^{-1} indicates the characteristics of the carboxyl functional group (C=O). The range between 1594-1418 cm^{-1} depicts the C-O symmetric stretch of the carboxyl group, and the presence of a C-O asymmetric stretch was identified at 1180.43 cm^{-1} [23]. The peak at 2945.3 cm^{-1} indicates intramolecular hydrogen bonds involving O-H and -COO- along with Ca^{2+} ions, while the peak at 3647.39 cm^{-1} represents O-H stretching vibrations especially in calcium alginate [24].

In the alginate-chitosan spectrum, there was a shift and the emergence of new functional groups due to the addition of chitosan. An important shift occurs at 3630.15 cm^{-1}, which indicates O-H stretching vibrations and N-H stretching vibrations, consistent with previous research by Venkatesan et al. [25]. The wider band at 2943.37 cm^{-1} indicates intramolecular bonds between O-H, -COO-, and Ca^{2+} ions together with the NH_2 group. The peak at 1186.22 and 1750.10 cm^{-1} indicates asymmetric C-O and C=O stretching. The characteristic peak at 1649.13 cm^{-1} represents the ketone C=O stretching vibration on primary NH_2, which indicates the presence of N-H bending which indicates interaction with the protonated amino group on chitosan. The wavenumber shift in the -OH group indicates an increase in energy level [26].

3.4. Characterization of calcium-based alginate-chitosan membrane using SEM

The calcium-based alginate-chitosan membrane that has been formed is analyzed for its microstructure using SEM (Scanning Electron Microscope) to examine the surface and pore diameter of the membrane. The SEM results obtained under optimal conditions can be observed in Figure 3.

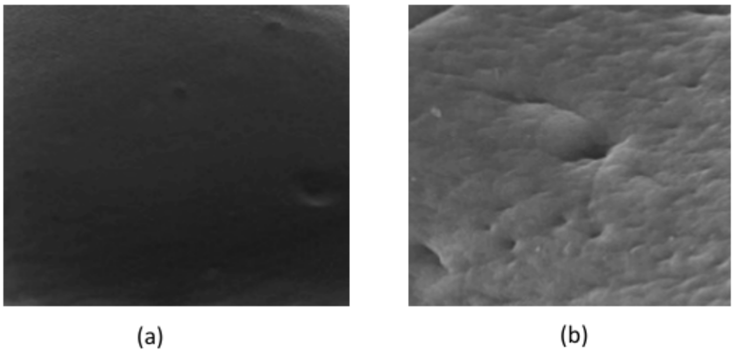

Figure 3. SEM analysis of a calcium alginate membrane at (a) 1000x (b) 5000x magnification.

Under 5000x magnification, the surface of the calcium alginate particles shows a considerable surface area, displaying a particle diameter of 138 nm. Smaller particle size correlates with expanded surface area, leading to increase adsorption rates. These characteristics place calcium alginate in the classification of microporous materials, as indicated by its particle size and is described in detail in this study [27]. Figure 4 illustrates the comparative analysis between various calcium alginate membranes.

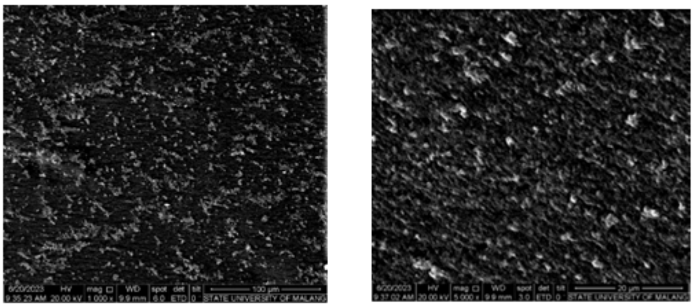

(a) (b)

Figure 4. SEM analysis of calcium alginate-chitosan membrane at (a) 1000x, (b) 5000x magnification.

SEM analysis findings at 5000x magnification show the inner surface structure of the membrane, which is characterized by roughness and porosity, with a diameter of 185.96 nm. This size classification aligns them with microporous membranes [27]. These membrane pores play an important role as adsorbents during NaCl adsorption, facilitating movement within the pore walls in the adsorption process.

3.5. Adsorption of NaCl using calcium-based alginate-chitosan membrane synthesis

3.5.1. Adsorption of NaCl using variation of alginate solution for optimization

Sodium alginate functions as the base material in gel formation along with Ca2+ from CaCl2, which cross-links with sodium alginate and chitosan. The optimization process focuses on identifying the most effective concentration of sodium alginate for adsorption purposes. This optimization phase involves testing membrane configurations utilizing sodium alginate solutions at concentrations of 1 and 2% w/v, combined with 1% w/v of chitosan. The quantities utilized consist of 26.6 mL of NaAlginate solution, 13.3 mL of chitosan solution, and 10 mL of 0.5 M CaCl2. The optimized condition of ideal composition is shown in Table 3, as follows:

Table 3. Optimized sodium alginate solution concentration form maximum adsorption.

Na-Alginate (ml; w/v)	Chitosan (vol; w/v)	Concentration (ppm) $[Cl^-]$ Initial	 $[Cl^-]$ Residue	 $[Cl^-]$ Adsorbed	%Adsorption
26.6; 1%	13.3; 1 %	3543	2290	1253	34.8
26.6; 2%	13.3; 1 %	3543	2130	1413	40.0
26.6; 3%	13.3; 1 %	3543	2330	1213	34.2
26.6; 4%	13.3; 1 %	3543	2370	1173	33.1

As listed in Table, the membrane containing a 2%w/v alginate concentration demonstrates a higher capacity for adsorbing Cl- ions compared to the 1% w/v alginate concentration membrane. The concentration of sodium alginate plays a crucial role in gel formation, influencing the density of particles within the solution. Higher concentrations lead to a denser presence of charges or particles, facilitating increased electrostatic interactions between more functional groups and the -NH3+ groups in chitosan. Consequently, this interaction enhances the membrane's capacity for substance adsorption [28].

3.5.2. Adsorption of NaCl using Variation of Chitosan for Optimized adsorption

The optimization of chitosan solution concentration is performed to determine the best membrane composition for further membrane application with contact time. The optimization data is listed in Table 4.

Table 4. Optimized Chitosan Solution for adsorption maximum.

Na-Alginate	Chitosan	Concentration (ppm)			%Adsorption
(ml ; w/v)	(ml ; w/v)	[Cl$^-$] Initial	[Cl$^-$]Residue	[Cl$^-$] Adsorbed	
26.6 ; 2%	13.3 ; 0 %	3542	2662	880	24.8
26.6 ; 2%	13.3 ; 1 %	3542	2130	1412	39.8
26.6 ; 2%	13.3 ; 2 %	3542	1846.0	1696	48.4
26.6 ; 2%	13.3 ; 3 %	3542	2378.5	1164	32.3

Table 4 shows the membrane incorporating chitosan exhibits superior performance due to the incorporation of active cross-linking agents, which leads to an increase in membrane pore size, thereby enhancing its capacity for adsorption. The alginate-chitosan composite membrane was presumed to demonstrate superior absorption of chloride ions (Cl-) up to 48.4%, and then decreasing of 32.3% with variation 2:3 between Na-Alginate and Chitosan composition.

The decrease in adsorption level at the 2:3 ratio of Na-alginate to chitosan may be due to the saturation of the chitosan solution, resulting in a decrease in the availability of active amino groups for cross-linking with alginate. This reduced the effective surface area for ion adsorption. Additionally, excess chitosan content possibly causes the formation of chitosan aggregates, which can hinder the formation of a uniform and stable membrane. The phenomenon of influenced chemical factors are related to the balance of ionic interactions between chitosan and alginate, as well as the availability of functional groups for cross-linking. An abundance of chitosan can disrupt this optimal interaction balance, resulting in a decrease in adsorption efficiency [29,30].

The process of combination between chitosan solution with alginate reveals in an interaction between the positively charged amino groups (-Nh3+) of chitosan and the -COO- groups of alginates through ionic interactions, establishing cross-linking bonds.

3.5.3. Adsorption of NaCl using the optimized condition

The utilization of the calcium alginate and chitosan as the membrane was assessed by adsorbing NaCl in the ranged from 10 to 50 minutes in the batch system. The outcomes of the membrane's work were measured in terms of the maximal percentage adsorption of Na+ and Cl-. The data of adsorption test of calcium alginate with addition chitosan in the membrane for Na+ adsorption is presented in Table 5.

Table 5. Analysis of the Na+ ion adsorption level by membrane using AAS.

Contact Time	Concentration (ppm)			%Adsorption
(Minutes)	[Na$^+$] Initial	[Na$^+$] Residue	[Na$^+$] Adsorbed	
10	1105	668	437	39.5
20	1105	693	411	37.2
30	1105	688	416	37.7
40	1105	657	447	40.5
50	1105	745	359	32.5

As listed in Table 5, the optimal time analysis towards the maxima Na+ ion adsorption is 40 minutes. The particle aggregation on the membrane potentially affected the adsorption of Na+ ions.

These ions are typically bound by -COO- groups originating from alginate, crucial in the NaCl adsorption process. The presence of -NH3+ groups from chitosan is suspected to contribute to this aggregation.

Figure 5 illustrates the correlation between contact time and the percentage of Na+ adsorption. This reveals a notable decline at the 50-minute. This implies a reduction in the membrane's adsorption capacity, potentially linked to a decrease in chitosan content or a decline in NH2 groups within the membrane. Chitosan's efficacy in binding metals stems from its free amino groups and integral for ion exchange capabilities. The nitrogen content in chitosan with its high polymer chain correlates with its capacity to bind metals.

As listed in Table 6, the ion Cl- adsorption test was utilized using the Mohr method. As listed in the table, it becomes evident that the optimal duration for Cl- ion adsorption is 40 minutes, the same with its pattern of Na+ ion. The contact time plays a vital role in the adsorption process, directly impacting the amount of adsorbed substance. The optimized contact allows for more solute molecules to be adsorbed, facilitating a well-functioning diffusion process [31]. It significantly influences adsorption until equilibrium is attained. Once equilibrium is reached, further contact time does not affect the process or possibly desorption.

Table 6. Analysis of the Cl- adsorption levels in the NaCl 0.1 N solution using the Mohr Method Argentometric titration.

Contact Time (Minute)	Concentration (ppm)			
	$[Cl^-]$ Initial	$[Cl^-]$ Residue	$[Cl^-]$ Adsorbed	%Adsorption
10	3543	1988	1554	43.9
20	3543	1952	1590	44.9
30	3543	1864	1661	47.4
40	3543	1828	1696	48.4
50	3543	1881	1661	46.9

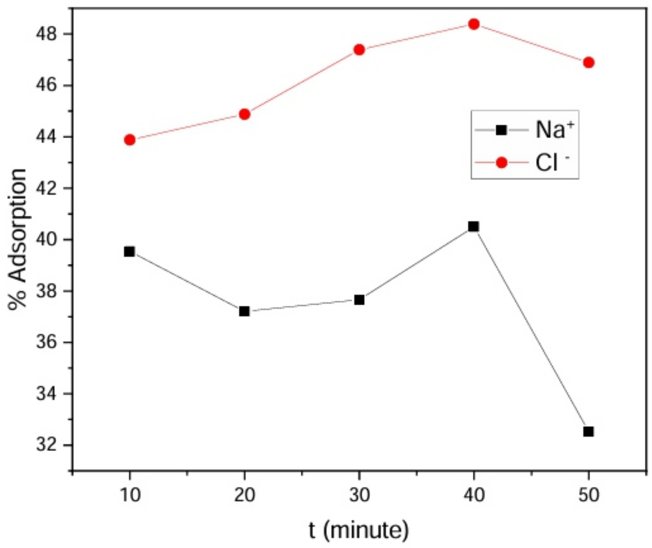

Figure 5. Relationship between contact time and the percentage of Na+ and Cl- ion adsorption.

Figure 5 indicates a substantial increase in the Na+ and Cl- ions adsorption process at 40 minutes, revealing them as the optimal time for both ions. Conversely, there is a decline in observing them at 50 minutes. Prolonging the process beyond 60 minutes could potentially lead to desorption, releasing the adsorbate back into the solution. Figure 5 depicts the graphical representation of the relationship between contact time and the percentage of Na+ and Cl- ions adsorption.

The possible mechanism reaction between Ca-alginate and chitosan during adsorption of Na+ and Cl- as shown in Figure 6, as follows:

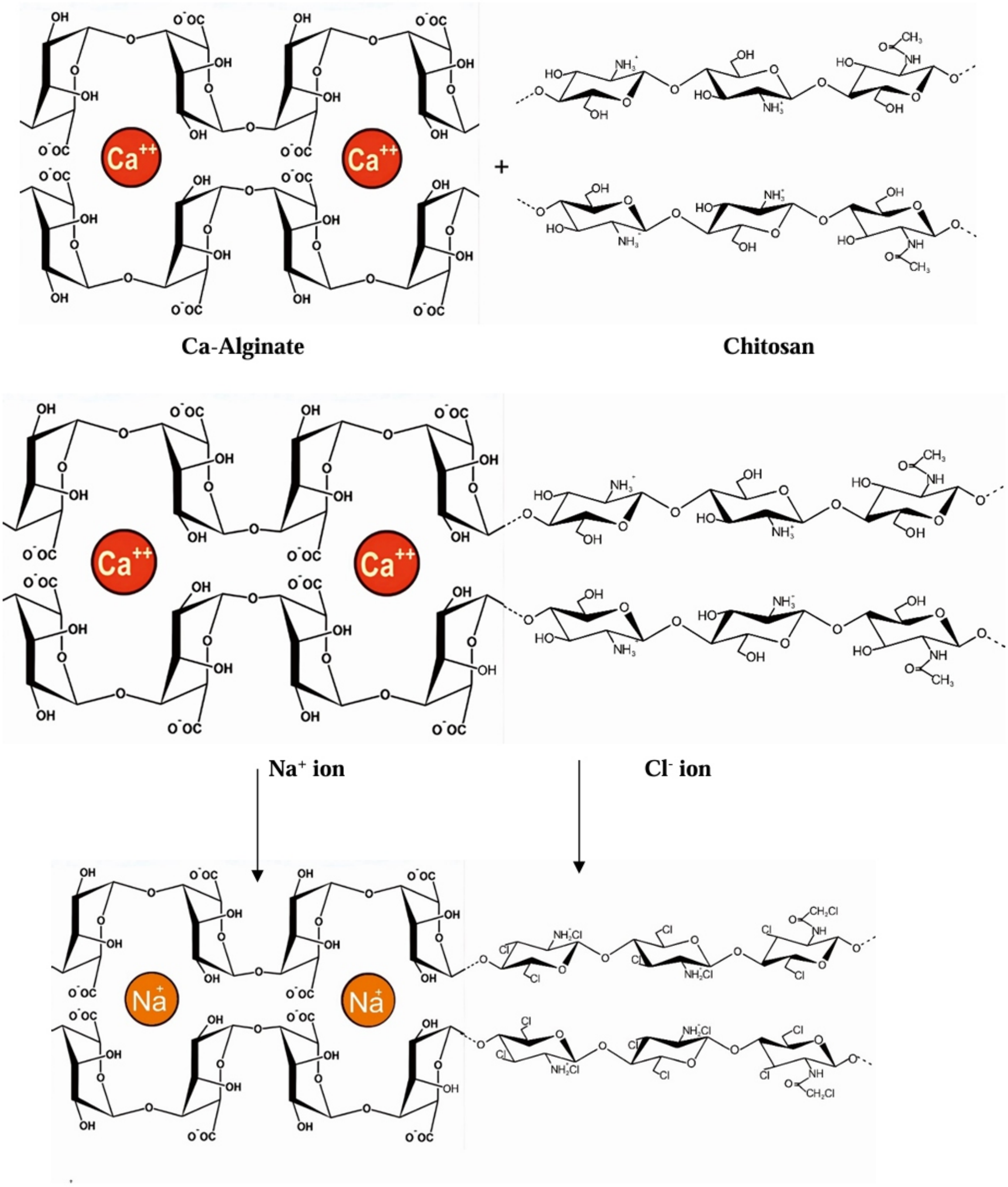

$$+ [Ca(OH)_2]_x + [Ca(OH)_2]_y......$$

Figure 6. The possible mechanism reaction between Ca-alginate chitosan with NaCl during the adsorption process.

The initial mechanism reaction started a reaction between Ca-alginate and chitosan to form a Caalginate-chitosan complex, causing the cross linking of the polymer to involve hydrogel formation for potentially adsorption application. During the adsorption, the first step involved the displacement of Ca2+ changing with Na+ ion due to the higher affinity of Na+ ion to alginate. The first product in the adsorption process was the dissolution of Ca complex and trapped Na-alginate chitosan in the membrane. In the second product, when the Cl- ion was applied in the adsorption process, chitosan could possibly interact with Cl- ions through electrostatic interactions, hydrogen bonding, and its positively charged amino groups attracted Cl- ions. The residue of this process adsorption formed a Ca(OH)2 complex. In the future prospect, the specific condition of pH and temperature between Caalginate chitosan and NaCl should be considered to determine the best capability membrane as adsorbent.

4. Conclusions

The inclusion of chitosan in calcium alginate had an impact on membrane formation, which was reflected in FTIR characterization by observing shifts in the wave numbers of certain functional groups. On the calcium alginate membrane, the absorption of the O-H group at 3647.39 shifted to 3437 cm-1, which indicated the existence of intramolecular bonds with the N-H group of chitosan. In addition, C=O, CO, and N-H groups were involved in NaCl binding. SEM analysis showed a particle size diameter of 185.96 nm, indicating rough and porous surface characteristics, indicating the microporous nature of the membrane, which is capable of absorbing NaCl. The calcium alginate-chitosan based membrane showed a Na+ and Cl- adsorption peak of 40.5% and 48.4%, respectively. This maximum adsorption level was achieved using a membrane composition consisting of 13.3 mL of 2% chitosan (w/v) and 26.6 mL. The optimized contact time for this Ca-alginate addition with chitosan was detected at 40 minutes to adsorb of Na+ and Cl- ions.

Use of AI tools declaration

The authors declare they have not used Artificial Intelligence (AI) tools in the creation of this article.

Acknowledgments

This research was funded by Penelitian Dasar grant No. 0162/E5.4/DT.05.00/2023 on DRPM 2023

Conflict of Interests

The authors state that there are no conflicts of interest for this project.

References

1. Bibi A, Ur-Rehman S, Akhtar T, et al. (2020) Effective removal of carcinogenic dye from aqueous solution by using alginate-based nanocomposites. Desalin Water Treatt 208: 386–398. https://doi.org/10.5004/dwt.2020.26432

2. Millero FJ, Feistel R, Wright DG, et al. (2008) The composition of Standard Seawater and the definition of the Reference-Composition Salinity Scale. Deep-Sea Res Part I-Oceanogr Res Pap 55: 50–72. https://doi.org/10.1016/j.dsr.2007.10.001

3. Armid A, Shinjo R, Takwir A, et al. (2021) Spatial distribution and pollution assessment of trace elements Pb, Cu, Ni, Fe and as in the surficial water of Staring Bay, Indonesia. J Braz Chem Soc 32: 299–310. https://doi.org/10.21577/0103-5053.20200180

4. Wijaya AR, Khoerunnisa F, Armid A, et al. (2022) The best-modified BCR and Tessier with microwave-assisted methods for leaching of Cu/Zn and their δ65Cu/δ66Zn for tracing sources in *marine sediment fraction. Environ Technol Innov 28.*

5. Wijaya AR, Kusumaningrum IK, Hakim L, et al. (2022) Road-side dust from central Jakarta, Indonesia: Assessment of metal(loid) content, mineralogy, and bioaccessibility. Environ Technol Innov 28: 102934. https://doi.org/10.1016/j.eti.2022.102934

6. Lachish U (2007) Optimizing the Efficiency of Reverse Osmosis Seawater Desalination. 1–17.

7. Honarparvar S, Zhang X, Chen T, et al. (2021) Frontiers of membrane desalination processes for brackish water treatment: A review. Membranes 11. https://doi.org/10.3390/membranes11040246

8. Piekarska K, Sikora M, Owczarek M, et al. (2023) Chitin and Chitosan as Polymers of the Future—Obtaining, Modification, Life Cycle Assessment and Main Directions of Application. Polymers 15. https://doi.org/10.3390/polym15040793

9. Zhang H, Li X, Zheng S, et al. (2023) The coral-inspired steam evaporator for efficient solar desalination via porous and thermal insulation bionic design. SmartMat 4: 1–12. https://doi.org/10.1002/smm2.1175

10. Cao DQ, Tang K, Zhang WY, et al. (2023) Calcium Alginate Production through Forward Osmosis with Reverse Solute Diffusion and Mechanism Analysis. Membranes 13: 1–15. https://doi.org/10.3390/membranes13020207

11. Nakayama R ichi, Takamatsu Y, Namiki N (2020) Multiphase calcium alginate membrane composited with cellulose nanofibers for selective mass transfer. SN Appl Sci 2: 1–7. https://doi.org/10.1007/s42452-020-03532-1

12. Long Q, Zhang Z, Qi G, et al. (2020) Fabrication of Chitosan Nanofiltration Membranes by the Film Casting Strategy for Effective Removal of Dyes/Salts in Textile Wastewater. ACS Sustain Chem Eng 8: 2512–2522. https://doi.org/10.1021/acssuschemeng.9b07026

13. Nalatambi S, Oh KS, Yoon LW (2021) Fabrication technique of composite chitosan/alginate membrane module for greywater treatment. J Physics Conf Ser 2120. https://doi.org/10.1088/1742-6596/2120/1/012037

14. Benettayeb A, Ghosh S, Usman M, et al. (2022) Some Well-Known Alginate and Chitosan Modifications Used in Adsorption: https://doi.org/10.3390/w14091353 A Review. Water 14: 1–26.

15. Thanakkasaranee S, Sadeghi K, Lim IJ, et al. (2020) Effects of incorporating calcined corals as natural antimicrobial agent into active packaging system for milk storage. Mater Sci Eng C 111: 110781. https://doi.org/10.1016/j.msec.2020.110781

16. Shahid MK, Mainali B, Rout PR, et al. (2023) A Review of Membrane-Based Desalination Systems Powered by Renewable Energy Sources. Water 15. https://doi.org/10.3390/w15030534

17. Kosanović C, Fermani S, Falini G, et al. (2017) Crystallization of calcium carbonate in alginate and xanthan hydrogels. Crystals 7: 1–15. https://doi.org/10.3390/cryst7120355

18. Milita S, Zaquin T, Fermani S, et al. (2023) Assembly of the Intraskeletal Coral Organic Matrix during Calcium Carbonate Formation. Cryst Growth Des 23: 5801–5811. https://doi.org/10.1021/acs.cgd.3c00401

19. Goffredo S, Vergni P, Reggi M, et al. (2011) The skeletal organic matrix from Mediterranean coral Balanophyllia Europaea influences calcium carbonate precipitation. PLoS ONE 6. https://doi.org/10.1371/journal.pone.0022338

20. Suci CW, Wijaya AR (2020) Analysis of fe in coral reefs for monitoring environmental areas of prigi coast waters using the tessier-microwave method. IOP Conf Ser Mater Sci Eng 833. https://doi.org/10.1088/1757-899X/833/1/012046

21. Suci CW, Wijaya AR, Santoso A, et al. (2020) Fe leaching in the sludge sediment of the prigi beach with tessier-microwave method. AIP Conference Proceedings 2231. https://doi.org/10.1063/5.0002589

22. Pavoni JMF, Luchese CL, Tessaro IC (2019) Impact of acid type for chitosan dissolution on the characteristics and biodegradability of cornstarch/chitosan based films. Int J Biol Macromol 138: 693–703. https://doi.org/10.1016/j.ijbiomac.2019.07.089

23. Daemi H, Barikani M (2012) Synthesis and characterization of calcium alginate nanoparticles, sodium homopolymannuronate salt and its calcium nanoparticles. Sci Iran 19: 2023–2028. https://doi.org/10.1016/j.scient.2012.10.005

24. Grossi A, De Laia S, De Souza E, et al. (2014) a Study of Sodium Alginate and Calcium Chloride Interaction Through Films for Intervertebral Disc Regeneration Uses. 21o CBECIMAT - Congresso Brasileiro de Engenharia e Ciência dos Materiais 7341–7348.

25. Venkatesan J, Bhatnagar I, Kim SK (2014) Chitosan-alginate biocomposite containing fucoidan for bone tissue engineering. Mar Drugs 12: 300–316. https://doi.org/10.3390/md12010300

26. Tang S, Yang J, Lin L, et al. (2020) Construction of physically crosslinked chitosan/sodium alginate/calcium ion double-network hydrogel and its application to heavy metal ions removal. Chem Eng J 393: 124728. https://doi.org/10.1016/j.cej.2020.124728

27. Hamedi H, Moradi S, Tonelli AE, et al. (2019) Preparation and characterization of chitosanAlginate polyelectrolyte complexes loaded with antibacterial thyme oil nanoemulsions. Appl Sci 9. https://doi.org/10.3390/app9183933

28. Permanadewi I, Kumoro AC, Wardhani DH, et al. (2021) Analysis of Temperature Regulation, Concentration, and Stirring Time at Atmospheric Pressure to Increase Density Precision of Alginate Solution. Teknik 42: 29–34. https://doi.org/10.14710/teknik.v42i1.35994

29. Lawrie G, Keen I, Drew B, et al. (2007) Interactions between alginate and chitosan biopolymers characterized using FTIR and XPS. Biomacromolecules 8: 2533–2541. https://doi.org/10.1021/bm070014y

30. Niculescu AG, Grumezescu AM (2022) Applications of Chitosan-Alginate-Based Nanoparticles—An Up-to-Date Review. Nanomaterials 12. https://doi.org/10.3390/nano12020186

31. Rina Tri Vidia Ningsih, Anugrah Ricky Wijaya, Aman Santoso Aman M (2023) Chitosan membrane modification using silica prigi Bay for Na+ ion adsorption. AIP Conf Proc 2634: 020014. https://doi.org/10.1063/5.0111964

Sustainable plastic bottle recycling: employing zinc-deposited SBA-15 as a catalyst for glycolysis of polyethylene terephthalate

Pailin Srisuratsiri1, Ketsarin Chantarasunthon1, Wanutsanun Sudsai1, Pichet Sukprasert1, Laksamee Chaicharoenwimolkul Chuaitammakit2,* and Wissawat Sakulsaknimitr1,*
1 Department of Fundamental Science and Physical Education, Faculty of Science at Sriracha,
Kasetsart University, Sriracha campus, Chonburi 20230, Thailand
2 Chemistry and Applied Chemistry, Faculty of Science and Technology, Suratthani Rajabhat
University, 272 Moo 9, Surat-Nasan Road, Khuntale, Muang, Surat Thani 84100, Thailand

ABSTRACT

Novel catalysts for recycling PET bottles into monomers have been developed by depositing zinc onto the surface of SBA-15, mitigating ZnO catalyst agglomeration in glycolysis separation processes to enhance reaction yields. Various zinc compounds (Zn(OAc)2, ZnCl2, and ZnSO4) were employed as substrates for catalyst design on the porous, high-surface-area material SBA-15 via impregnation. The presence of distinct Zn species on SBA-15 was confirmed through XRD and EDS analyses. The acidity of the catalyst, a crucial factor in the PET glycolysis process, was assessed using different Zn-containing precursors. NH3-TPD measurement has revealed the highest acidity in ZnCl2, followed by Zn(OAc)2 and ZnSO4, respectively. Glycolysis reactions with a PET:EG ratio of 1:5 and a 1% catalyst at 200°C for 2 hours revealed the catalytic efficacy of zincdeposited compounds in the sequence ZnCl2 > Zn(OAc)2 > ZnSO4. Surprisingly, the ZnCl2 catalyst produced the highest yield of bis-2-hydroxyethyl terephthalate (BHET) at 75% and displayed exceptional recycling capability over three cycles, contributing significantly to resource recovery objectives aligned with the Sustainable Development Goals (SDGs).

Keywords: sustainable development goals; glycolysis; SBA-15; Zn catalyst; polyethylene terephthalate

1. Introduction

Polyethylene terephthalate (PET) is widely used for beverage packaging due to its exceptional properties, including transparency, gas and water resistance, high impact strength, UV resistance, and being lightweight. However, the global production and use of PET bottles have led to significant plastic waste, causing environmental pollution and reducing landfill space. Incineration as a waste management method not only generates energy but also contributes to air pollution. The Great Pacific Garbage Patch serves as a clear example of the negative impacts of plastic waste on a global scale, breaking down into microplastics that contaminate soil, water, and air. Studies have even found microplastics in seafood and human blood, which have been linked to respiratory problems and the development of cancer [1]. Additionally, the production of PET bottles relies on fossil fuels, contributing to greenhouse gas emissions and climate change. Therefore, immediate action is essential to address and prevent this issue from escalating into a worldwide public health and environmental crisis.

Recycling is a promising way to reduce waste in landfills. Various methods can be employed to recover PET, including primary (re-extrusion), secondary (mechanical), tertiary (chemical), and quadruple (energy recovery) methods that possess their own advantages and disadvantages in terms of cost, quality, and environmental impact. For primary and secondary methods, the properties of recycled-grade PET deteriorate by thermal degradation during the process due to contamination of acid, water, color, and additives in the plastic [2]. Chemical recycling, on the other hand, involves breaking down polymer chains into monomers, providing valuable feedstock for the plastic industry, and promoting a circular economy. Among the chemical recycling reactions, glycolysis has gained significant attention due to its moderate operating temperature, mild reagents, normal pressure, high yield, and scalability. Glycolysis involves the trans-esterification of PET polymers using glycols, primarily ethylene glycol (EG), resulting in the cleavage of ester linkages to obtain bis-2hydroxyethyl terephthalate (BHET) [3].

However, without a catalyst, the glycolysis of PET is inherently slow. This is primarily because the adjacent aromatic ring in the PET structure stabilizes the carbonyl group, which has a low degree of reactivity. Zinc acetate (Zn(OAc)2) is widely used as a catalyst in PET glycolysis, offering a high yield of BHET compared to other metal salts. Nevertheless, its drawback lies in the dissolution of the metal salt in EG, making it challenging to recover for reuse. Even trace amounts of metal ions remaining in the BHET monomer can adversely affect the properties of the polymer, including rheological behavior, discoloration, and degradation of polymer chains [2,4]. While solid catalysts composed of metal oxide particles, mostly transition metals, have been used, their toxicity poses significant risks to the environment. Zinc oxide (ZnO), a non-toxic metal oxide commonly found in sunscreen [5], presents a promising alternative. It is not only environmentally friendly, but also exhibits excellent catalytic potential. Previous studies have investigated the reactivity of ZnO in PET glycolysis, showing a high yield of BHET but requiring high operating temperatures and pressures (260 °C and 5 atm) [6]. Our work explored the use of ZnO nanoparticles via reflux under normal pressure to achieve a high yield of BHET [7], although the aggregation of nanoparticles after use reduces the efficiency of the reaction acceleration.

Furthermore, nanoparticles may mix with the wastewater used for BHET washing, potentially leading to environmental contamination that could impact living organisms. To address this issue, distributing the catalyst on the surface of a support material could be offered. Santa Barbara Amorphous-15 (SBA-15) is a mesoporous silica with a uniform hexagonal pore, a narrow pore-size distribution, and a high surface area. It has been applied to be a supported material for ZnO to utilize in various applications, including photocatalytic degradation [8,9], antibacterial agents [10], and catalysts [11–13]. For instance, Bhuyan et al. successfully prepared a ZnO/SBA-15 catalyst for the synthesis of dihydropyrimidinones. The catalytic efficiency of the ZnO nanocomposite was superior to that of pure ZnO nanoparticles, requiring a lower catalyst loading and a shorter reaction time [11]. Yao et al. employed ZnO/SBA-15 for the glycolysis of PET, achieving a remarkable 91% yield of BHET. The authors also noted that the resulting product exhibited improved whiteness compared to catalysts such as Zn(OAc)2, ZnO, and ionic liquids [14].

The role of zinc in the glycolysis reaction was studied and generally proposed at the acid site of the catalyst. Both zinc atoms and zinc ions (Zn2+) possess the ability to activate the carbonyl group of PET, facilitating its reaction with EG. However, most of the solid catalysts described in the literature for the glycolysis of PET are composed of metals or metal oxides. In a notable study, Datta and Pasha reported the preparation of ZnCl2 absorbed on silica for the synthesis of 4-methylcoumarins.

Their results demonstrated that Zn2+ ions on the silica surface could catalyze the reaction and be reused up to five times without a significant loss in efficiency [15].

The objective of this research is to develop catalysts comprising Zn2+ ions and ZnO distributed on SBA-15 for the purpose of catalyzing the glycolysis of PET waste bottles. Metal salts, namely Zn(OAc)2, ZnCl2, and ZnSO4, were introduced using a wet impregnation technique. The calcination temperature was maintained at a constant 550°C to prevent any alterations to the pore structure caused by excessive heat [10]. At this temperature, the Zn salts decompose in different ways, resulting in the formation of either ZnO or Zn2+ ions on the SBA-15 support material [16,17]. Subsequently, the prepared catalysts underwent characterization and were employed in the glycolysis of PET to investigate their efficiency and optimize reaction conditions.

2. Materials and methods

2.1. Materialss

The disposal PET bottles were collected, removed labels, and cleaned with detergent, then airdried and cut into chips (size 0.3 × 0.3 cm), avoiding the adhesive area. The chips were pulverized using a rotary cutter to obtain a PET particle size of 0.1 mm, further dried at 60 °C in an oven to remove moisture, and stored in a zip bag. Pluronic P123 (copolymer), tetraethyl orthosilicate (TEOS), 37% w/w hydrochloric acid (HCl), zinc acetate (Zn(OAc)2), zinc chloride (ZnCl2), zinc sulfate (ZnSO4), 95% ethanol, and ethylene glycol (EG) were analytical grade and used as received.

2.2. Synthesis of SBA-15

A Pluronic P123 solution was prepared by adding 4.0 g of Pluronic P123, 90.0 g of distilled water, and 60.0 g of 4 M HCl in a round-bottom flask. The mixture was stirred at room temperature for 2 hours until it was fully dissolved. Then, 8.5 g of TEOS was gradually added dropwise to the mixture while continuously stirring at 40 °C for 20 hours. The mixture was poured into the autoclave with the temperature controlled at 100 oC for 24 hours in an oven. After finishing the reaction, the autoclave was cooled to room temperature by soaking in water. The precipitate was filtered using vacuum filtration, washed thoroughly with 95% ethanol to remove the copolymer, and oven-dried at 100 °C for 24 hours. The resulting solid was calcine at 550 °C with a heating rate of 10 °C/min for 6 hours to obtain a white solid of SBA-15.

2.3. Synthesis of Zn/SBA-15

SBA-15 was added to the solutions of Zn(OAc)2, ZnCl2, or ZnSO4 by controlling the concentration of Zn at 10% wt. The mixture was impregnated at room temperature for 7 days. The precipitate was filtered using vacuum filtration, washed with distilled water, and dried at 100 °C for 24 hours. The resulting solid was calcine at 550 °C with a heating rate of 10 °C/min for 6 hours to obtain the expected Zn2+ or ZnO distributed on SBA-15 support. The prepared catalysts doped by Zn(OAc)2, ZnCl2, and ZnSO4 were designated as ZA, ZC, and ZS, respectively.

2.4. Glycolysis of PET plastics

PET particles were mixed with EG at a weight ratio of 1:5 in a digestion tube. The catalysts, calculated as a percentage of the weight of PET, were then added, and the mixture was heated in a digestion box for a specified period. The obtained mixture was filtered using the Büchner funnel and washed with hot distilled water to separate the catalyst and incomplete depolymerized PET. Distilled water was added to the filtrate and stirred using a magnetic bar for 45 minutes to dissolve EG from the product. Then, water was removed using a rotary vacuum evaporator until the volume of the remaining mixture was about 60 cm3. The mixture was transferred to a conical flask, closed with parafilm, and then placed in a refrigerator (4 °C) for 24 hours to crystallize BHET. The white solid of BHET was filtered using a Büchner funnel and washed with cold distilled water several times. The product was placed in an oven at 60 °C for 24 hours. The weight of BHET was recorded for calculating the percent yield of BHET (%YBHET) as in the equation below.

$$\%\mathrm{Y}_{\mathrm{BHET}} = \frac{\text{mol BHET}}{\text{mol PET}} \times 100$$

Where mol BHET is the weight of BHET divided by a molecular weight of BHET (254 g/mol) and mol PET is the weight of PET divided by a molecular weight of the repeating unit of PET (192 g/mol).

2.5. Characterization

The prepared catalysts were characterized by X-ray diffraction (XRD) (Rigaku, smart lab) to obtain the crystal information of the catalysts. Surface morphology and 2D projection pictures were examined by a field emission scanning electron microscope (SEM-Hitachi; SU-8030) equipped with Energy-dispersive X-ray spectroscopy (EDS) to determine the percentage of elements on the surface. A transmission electron microscope (TEM-Hitachi HT7700) was applied to explore the pore structure of SBA-15 and the lattice fringe of the Zn catalyst on the surface. Surface area, pore volume, and pore diameter were examined by the physisorption of N2 molecules using a BET analyzer (Micromeritics, 3Flex). The chemical functional group was confirmed using Fourier transform infrared spectroscopy (Jasco; FT-IR4000). The chemical state information from the surface of the catalysts was revealed by X-ray photoelectron spectroscopy (AXIS Ultra DLD). Temperature-programmed desorption (NH3-TPD) experiments on the catalysts were carried out using a TA instrument (SDT2960 Simultaneous DTA-TGA Universal 2000). Differential scanning calorimetry (DSC, Netzsch DSC 214 polyma) was applied to confirm the purity of BHET products.

3. Results and Discussion

3.1. Characterization of the catalysts

3.1.1. Chemical structure

The XRD spectra of the samples reveal intriguing findings. Figure 1 presents a broad peak within the 15-40 2-theta range, indicating the presence of amorphous silica. The distinctive peak pattern of ZnO wurtzite was observed in the ZA within the 2-theta range of 30-70. The signals of the ZS spectrum correspond to the crystalline structure of ZnSO4 H2O [pdf card No: 01-074-1331], indicating the unchanged nature of the ZnSO4 precursor. These observations can be attributed to the different decomposition temperatures of the various zinc salts, where Zn(OAc)2 decomposed at 280°C, ZnCl2 at 500°C, and ZnSO4 at 680°C, respectively [11,13]. Consequently, the experimental calcination temperature set at 500°C was exclusively adequate for the transformation of Zn(OAc)2 to ZnO. Nonetheless, the applied temperature might have been sufficient for ZC transformation, but the heating time possibly fell short of completely decomposing ZnCl2 into ZnO. Accordingly, it is plausible that the size of the ZnO crystallites was too small to be detected by the XRD technique. As for ZC, the applied temperature might have been sufficient, but the heating time possibly fell short of completely decomposing ZnCl2 into ZnO. Consequently, it is plausible that the size of the ZnO crystallites was too small to be detected by the XRD technique [10,18].

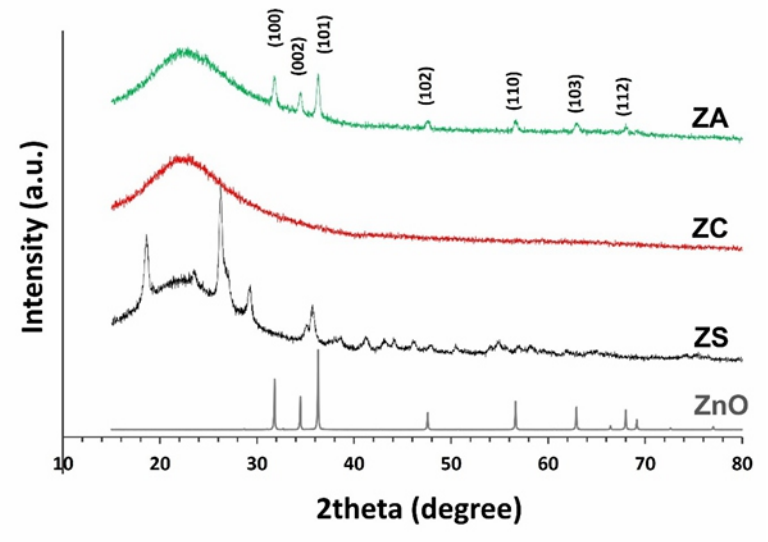

Figure 1. XRD patterns of the catalysts, prepared by impregnation and calcination at 550 °C.

Figure 2 displays the FTIR spectra of all the samples. The weak broad peaks at wavenumbers 3454 cm-1 (stretching and bending vibrations in the O−H bonds of silanol groups (Si−O−H)) and 1639 cm-1 suggest the residual adsorbed water molecules [19]. The relatively weak intensity of the O−H signal indicates a low level of O−H functionality on the surfaces of the samples. Notably, a strong broad peak within the range of 1280-1000 cm-1 and a weak peak at 800 cm-1 correspond to the asymmetric and symmetric stretching vibrations of Si−O−Si, and the prominent signal at 460 cm-1 pertains to the bending vibration of Si−O−Si, respectively. Additionally, a minor peak at 965 cm-1 was attributed to the asymmetric stretching of Si-OH [20]. Surprisingly, the characteristic ZnO signal at 400 cm-1 disappeared for the catalyst samples, indicating a limited presence of the catalyst on the surface of SBA-15.

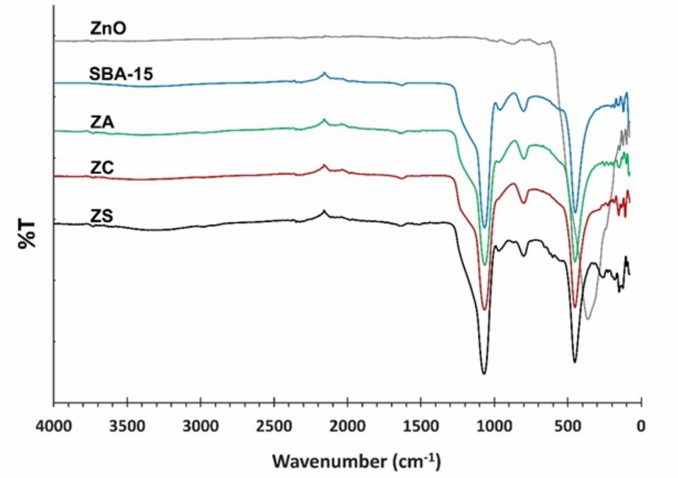

Figure 2. FTIR spectra of the commercial ZnO, SBA-15, and the catalysts.

3.1.2. The chemical state information from the surface

The XPS technique was employed to investigate the type of Zn atoms presenting on the surface of SBA-15, with their respective binding energies (BE) documented in Table 2. Intriguingly, the binding energy of Zn (2p3/2) in all samples was observed to be higher than that of pure ZnO (1021.11022.0 eV) [21–24]. This discrepancy could be attributed to the interaction between the Zn atom and silica through the formation of a Si−O−Zn bond. The difference in electronegativity between Si atoms (1.90) and the Zn atom (1.65) resulted in electron withdrawal from the Zn atoms.

Consequently, the reduction of electron density in the Zn atom contributes to a higher shift in its binding energy [21].

In the case of ZA, the Zn(2p) signal was detected at 1022.17 eV, which closely aligns with the binding energy of the pure ZnO, providing solid evidence for the presence of ZnO crystalline structures [21,25]. On the other hand, the Zn(2p) signal observed in ZS exhibited a higher energy value of 1023.02 eV, indicating a significant deviation of 0.88 eV from the pure ZnO. This variation could be attributed to the presence of Zn2+ ions with the characteristic Zn(2p) signals ranging from 1022.54 to 1023.07 eV [4,26], indicating their interaction with SBA-15. These findings further confirm the specific type of the presented Zn atoms and are consistent with the results obtained from the previous analytical techniques. The Zn(2p) signal of ZC was found at 1022.71 eV, which was greater than that of ZA. ZC spectra also showed a slight signal around 200 eV, corresponding to the Zn–Cl(2p3/2) and ZnCl(2p1/2) species [23]. These results implied that the prepared catalysts contain ZnO and Zn2+ ions on the surface of the ZC sample. In addition, the energy difference of 23 eV between the Zn(2p3/2) and Zn(2p1/2) signals serves as a characteristic indicator of the presence of ZnO in both ZA and ZC samples.

Table 2. Binding energy of the Zn atom from the XPS technique.

Samples	Zn($2p_{3/2}$)	Zn($2p_{1/2}$)	Different BE
ZA	1022.17	1045.22	23.05
ZC	1022.71	1045.74	23.03
ZS	1023.02	1046.13	23.12

3.1.3. Morphological and elemental analysis

SEM and EDS analyses provided insights into the surface morphology and elemental composition of the samples, as illustrated in Figure 3 and Table 1. The surface roughness of the Zncontaining catalysts exhibited a resemblance to that of SBA-15. Notably, chlorine and sulfur atoms were detected on ZC and ZS, indicating an incomplete decomposition of ZnCl2 and ZnSO4 into ZnO.

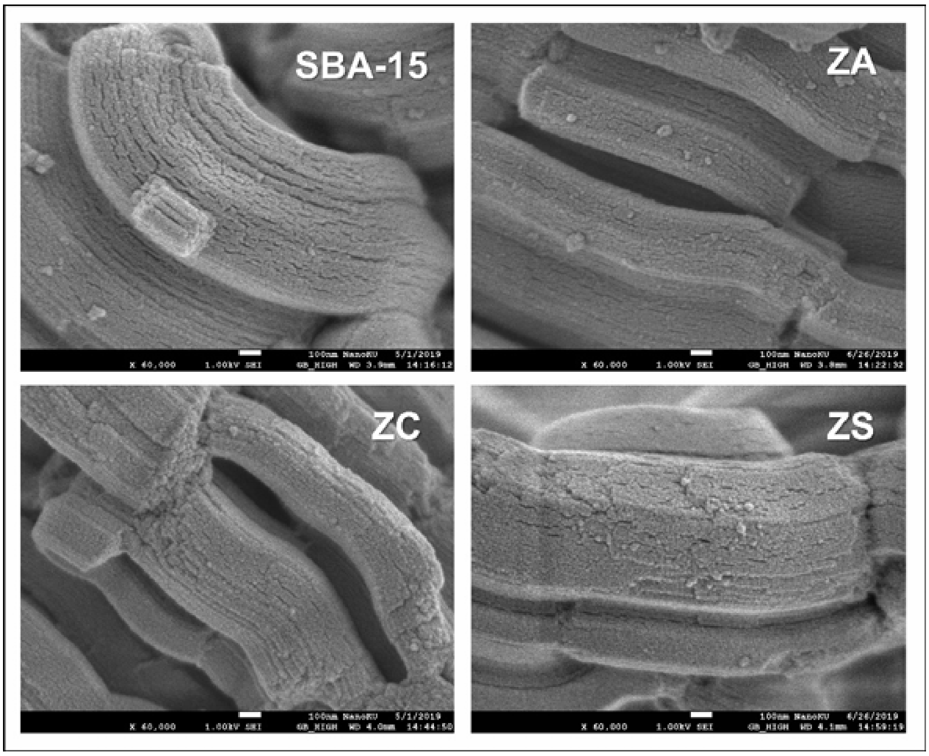

Figure 3. Surface morphology of the samples investigated by SEM.

Table 1. Atomic composition on the surface of the samples investigated by the EDS technique.

Samples	Elemental composition (Atomic%)					
	O	Si	Zn	Cl	S	others
SBA-15	80.64	19.36	-	-	-	-
ZA	76.54	20.59	2.29	-	-	0.58
ZC	77.11	18.91	2.90	1.08	-	-
ZS	77.35	16.93	1.92	-	2.37	1.43

TEM images (Figure 4) depict a remarkable two-dimensional hexagonal and honeycomb structure with long-range ordered channels, featuring a pore diameter ranging from 6 to 8 nm. Notably, the ZA sample showcases the presence of aggregated ZnO particles on the surface of SBA15. Upon closer inspection, the magnified image reveals the distinct parallel lattice fringes with a width of 0.28 nm, which corresponds to the (100) crystal face. In contrast, the ZS sample displays lattice fringes characteristic of ZnSO4, while the ZC sample exhibits no discernible features apart from SBA-15. These TEM findings align perfectly with the XRD data, reinforcing the consistency of the results.

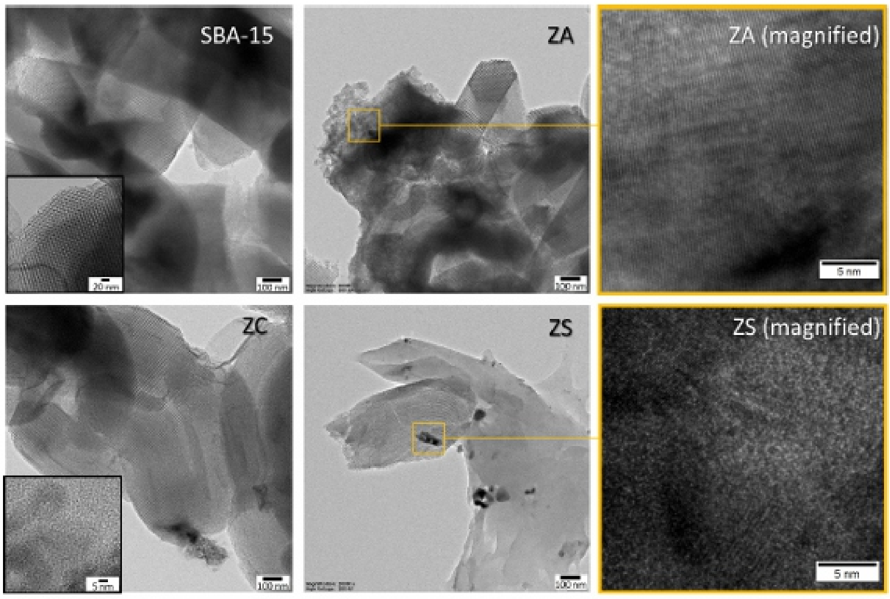

Figure 4. TEM images of SBA-15 and the catalyst samples. The scale bars of SBA-15, ZA, ZC, and ZS are 100 nm.

3.1.4. Surface area analysis

To assess the absorption characteristics of the sample, nitrogen adsorption/desorption isotherms were employed, providing useful insights into the surface area, pore volume, and pore size, as outlined in Table 3. Remarkably, all isotherms exhibited Langmuir type IV adsorption behavior, while the hysteresis branches with near-parallel alignment indicated the presence of cylindrical pores with a relatively consistent pore size [27]. Notably, the Zn-containing catalysts displayed a significant reduction in both BET-specific surface area and pore volume. Interestingly, the reduction in surface area surpassed the decline in pore volume, resulting in an overall increase in pore diameter compared to the SBA-15.

Table 3. Surface area, pore volume, and pore diameter of SBA-15 and prepared catalysts.

Samples	BET Surface area (m^2/g)	BJH (Desorption)		
		Surface area (m^2/g)	Pore volume (cm^3/g)	Pore diameter* (nm)
SBA-15	651.41	550.18	0.88	6.39
ZA	333.37	390.76	0.72	7.32
ZC	291.26	346.86	0.65	7.46
ZS	289.34	304.29	0.59	7.70

*Pore diameter is calculated using BJH (desorption) as 4V/A (V = pore volume and A = surface area). The data was calculated from the raw data of surface area and pore volume with 4 and 6 decimal places, respectively.

3.1.5. Acidity of the catalysts

The acidic properties of the samples were assessed using NH3-TPD (Figure 5). NH3 desorption temperature indicated acid site strength: weak (T < 200 °C), moderate (200 °C < T < 500°C), and strong

(T > 500°C) [28]. SBA-15 had limited acidic sites, with a broad desorption peak suggesting weak to moderate acidity. Incorporating Zn into SBA-15 increases acidic sites. ZA (ZnO) showed weak acidity at 160 °C and broad moderate acidity (200−400 °C) [29]. ZS (Zn2+) exhibited a distinct desorption peak at 238 °C, indicating moderate acidity [30]. These findings align with the literature on ZnO/S-1 and Zn2+/S-1 [25]. ZC provided the highest acidic site concentration, suggesting the coexistence of ZnO and Zn2+ ions. The total acidity trend is in the order of ZC > ZA > ZS > SBA15.

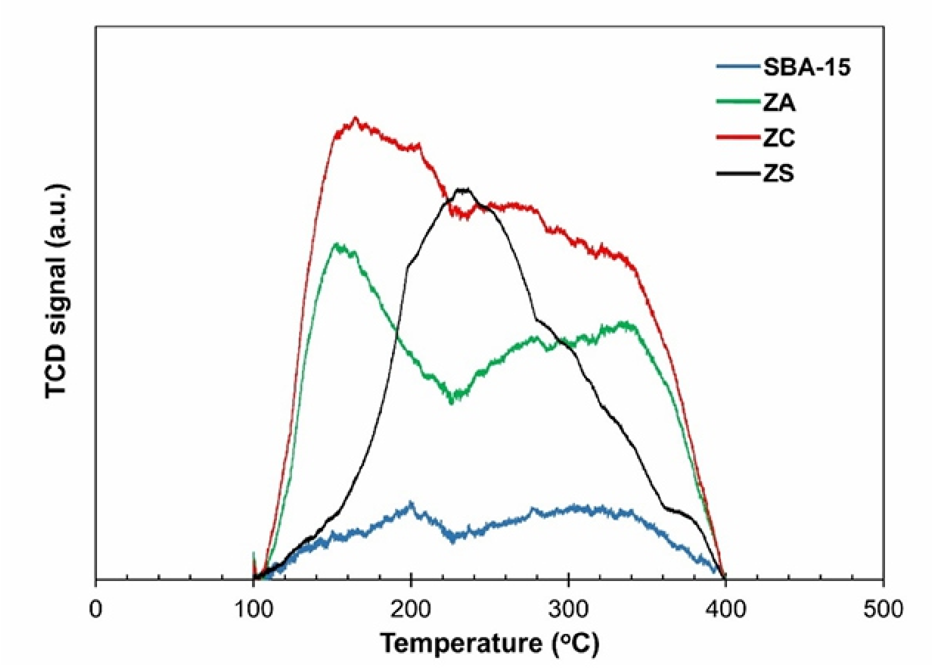

Figure 5. NH3-TPD profiles of SBA-15 and the catalysts.

3.2. Glycolysis of PET

SBA-15 and the catalysts were tested for PET glycolysis to evaluate their efficiency in recovering the BHET monomer. The catalyst at 1% (w/w) of PET was added to the PET:EG with a 1:5 (w/w) ratio at a constant temperature of 200°C. In the presence of catalysts, the %yield of BHET (%YBHET) rapidly increased within the first hour, followed by a gradual increase, and remained stabilized after 2 hours (Figure 6). Catalyst reactivity is in the order of ZC > ZA > ZS, which is correlated to their acidity. On the contrary to the zinc-deposited catalysts, SBA-15 exhibited no changes in the starting material after 3 hours due to the insufficiency of its acidity. Even with a small amount of Zn (1−3% atomic ratio) on the surface of SBA-15, the glycolysis reaction could be activated, yielding a higher amount of BHET compared to 15 of pure ZnO [7]. Consequently, ZC was selected for further optimization of PET glycolysis conditions.

The increase in catalytic efficiency can be attributed to the enhanced surface area of the active site. This suggests that the prepared catalysts exhibit a well-distributed Zn active site on the surface of SBA-15, which prevents agglomeration compared to the use of ZnO nanoparticles. Another contributing factor is the binding of Zn atoms to SBA-15, which enhances the acidity of the active site. The higher electronegativity of Si atoms compared to Zn atoms results in electron withdrawal from Zn atoms, increasing electrophilicity to accept electron pairs from carbonyl groups. Furthermore, in our research, we employed a digestion tube for PET glycolysis without additional stirring or dispersing techniques for the catalyst. During the reaction, EG vaporizes and condenses within the digestion tube. Reflux occurs when the temperature surpasses the boiling point of EG (197°C). After 2 hours, the reaction reaches equilibrium, yielding a constant BHET yield. This glycolysis method is easy to set up, employing mild reagents and requiring only an available heating source, making it suitable for potential large-scale applications.

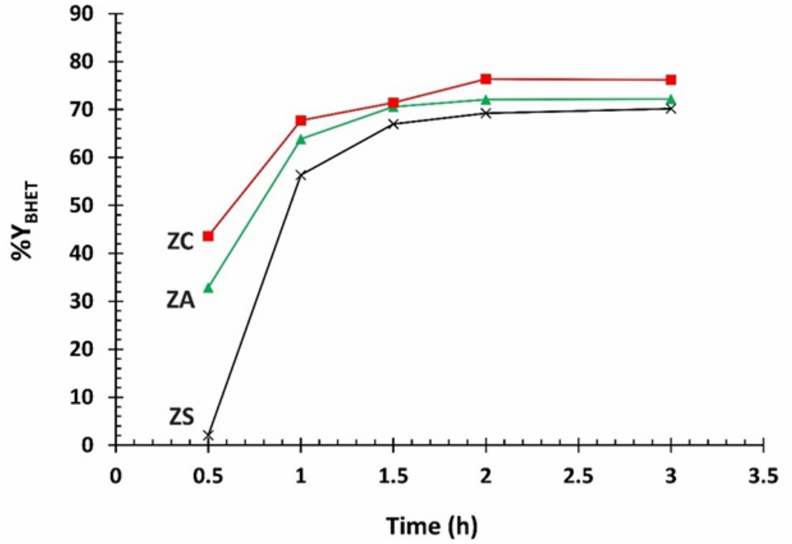

Figure 6. Efficiency of prepared catalysts on the glycolysis of PET. The reaction condition is the ratio of PET:EG (1:5) with a 1% catalyst at 200 °C.

To optimize the level of each parameter, a scanning experiment using ZC as the catalyst was conducted. Figure 7 illustrates that %YBHET consistently increased across all experiments. The PET:EG ratio of 1:5 was found to be adequate for the reaction, as previously reported [7]. The cost of chemical compounds was minimized by exploring the optimization range of 1:3 to 1:5. %YBHET remained constant at a temperature of 200°C and a catalyst concentration of 1%. Consequently, we conducted glycolysis experiments with 0.5−1.5% catalysts, temperatures ranging from 180−220°C, and durations of 1−2 hours, each with three replicated runs.

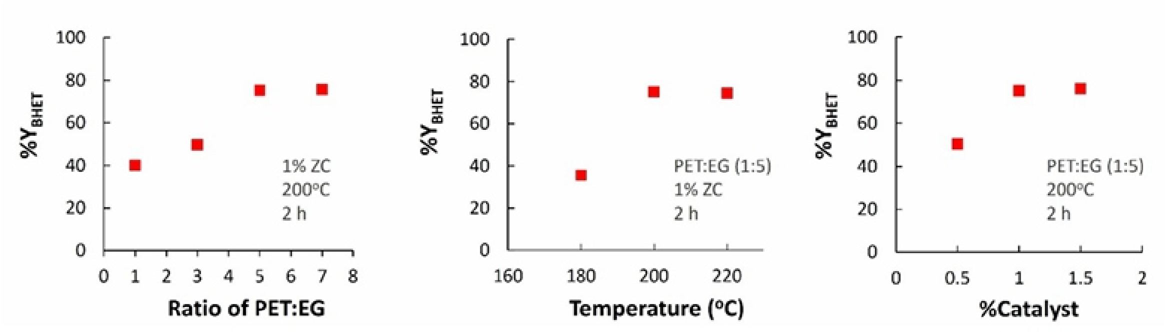

Figure 7. The scanning experiment to estimate the level of each parameter for the optimization.

Figure 8 presents the results of the optimized experiment. Temperature has a significant impact on %YBHET. At a temperature of 180°C, all conditions resulted in a product yield of less than 50%, likely due to glycolysis being a diffusion-controlled kinetic reaction [31]. The softening point of PET occurs at 220°C, and it is speculated that a solvent like EG can lower this point, facilitating faster depolymerization. The reported temperature for glycolysis of PET with EG is approximately 197°C (the boiling point of EG) or higher. Increasing the EG content greatly enhances glycolysis at lower reaction temperatures, but its effectiveness diminishes at 200°C and 220°C. The addition of catalyst from 1% to 1.5% slightly improves %YBHET. Glycolysis for a duration of 2 hours yields over 70% of the product, as summarized in Table 5. Based on these findings, we optimized the glycolysis conditions using a 1:5 PET:EG ratio and a 1% ZC catalyst at 200°C for 2 hours, resulting in a 75% yield of BHET.

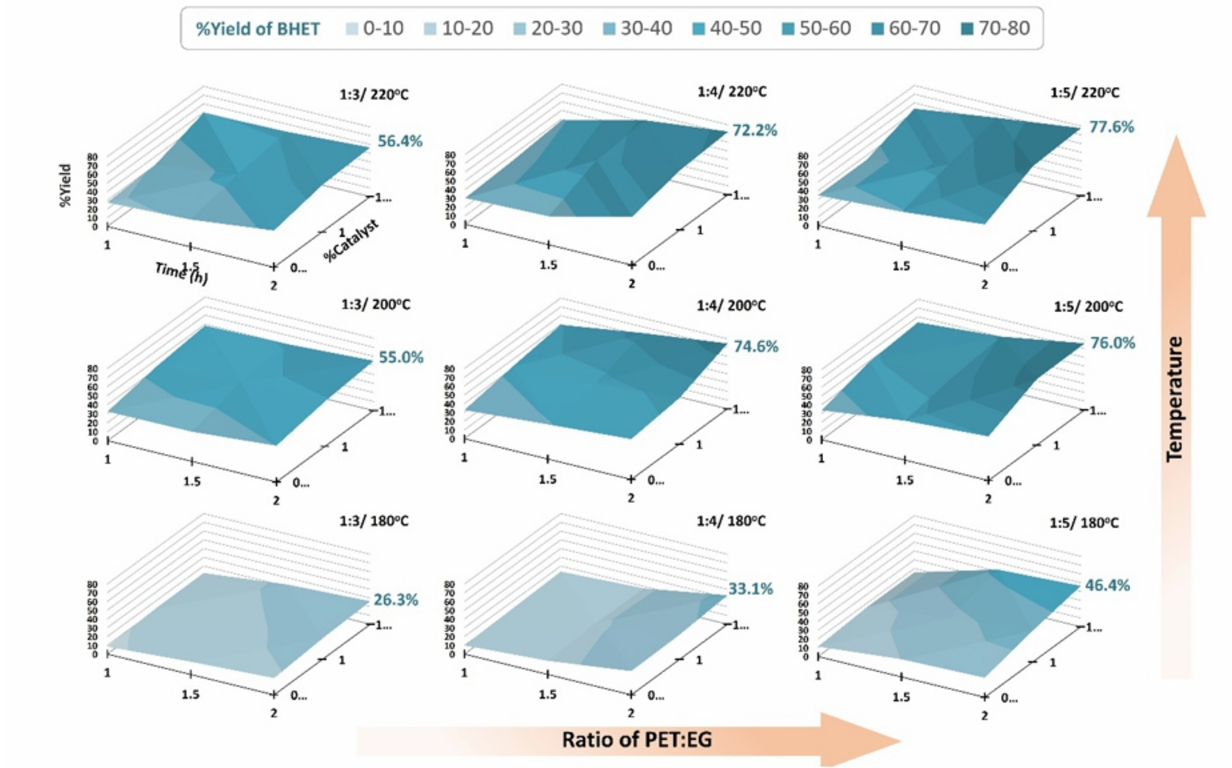

Figure 8. 3D graph for optimization of the parameters for glycolysis of PET using a ZC catalyst.

3.3. Purity of the BHET product

The FTIR spectrum of BHET displays prominent absorption peaks corresponding to the hydroxyl group (O−H) and carbonyl group (C=O) at wavenumbers of 3492-3432 cm-1 and 1713 cm1, respectively. The C−O stretching vibration signal was observed at 1270 cm-1. The methylene group is identified by stretching signals at 2954−2904 cm-1 (C−H stretching of methylene) and a bending signal at 1408 cm-1 (C−H bending). The presence of the aromatic ring is confirmed by the signals at 3090 cm-1 (C−H stretching of unsaturated carbon), 1650−1629 cm-1 (C=C stretching of aromatic ring), and 730 cm-1 (1,4-disubstituted benzene ring), respectively. The FTIR spectrum of the obtained BHET closely resembles that of the BHET standard, confirming the purity of BHET obtained from our glycolysis reaction (see SI, Figure S1).

The purity of the BHET product was also further assessed using melting point and DSC analysis. Our product exhibited a melting point range of 107−110°C, consistent with the reported standard value [7,32]. The DSC thermogram, spanning a range of 30−200°C, displayed a single sharp endothermic peak at 111°C, with no indication of a dimer by product signal (170°C) [33]. These findings confirm the purity of the BHET obtained from the glycolysis process (see SI, Figure S2).

3.4. Reusability

The ZC catalyst can be recovered by filtration, followed by washing with hot distilled water and drying at 80°C for 6 hours. By recycling the catalyst three times, the producibility of the BHET remained at 70% [11,15] (see SI, Figure S3).

4. Conclusion

Impregnating SBA-15 with various zinc salts and calcining at 550°C yielded active sites in the form of ZnO and Zn2+ ions. The presence of Zn atoms led to a decrease in surface area and pore volume compared to bare SBA-15. XRD and XPS analysis confirmed the presence of ZnO, ZnO/Zn2+, and Zn2+ in ZA, ZC, and ZS, respectively. The efficiency of catalysts in glycolysis has depended on their acidity, which is in the order of ZC > ZA > ZS >> SBA-15. Using a PET:EG ratio of 1:5, a 1% ZC catalyst based on the weight of PET, and heating at 200 °C for 2 hours resulted in the highest yield of BHET at 75% via recrystallization. The catalysts are conveniently prepared, reusable, and environmentally friendly. The catalyst we developed has the potential to be further enhanced in the future to enable industrial-scale PET bottle degradation. This work has implications for resource recovery and the circulation of BHET monomers in the PET industry, aligning with the goal of sustainable development.

Use of AI tools declaration

The authors declare that they have not used Artificial Intelligence (AI) tools in the creation of this article.

Acknowledgements

This work was supported in part by Kasetsart University Research and Development Institute (KURDI): R-M 26.62 and the Faculty of Science at Sriracha, Kasetsart University Sriracha campus. All are gratefully acknowledged for partial support and research facilities. Co-workers from the Faculty of Science and Technology, Suratthani Rajabhat University for supporting the chemical test equipment and laboratory area. Pailin Srisuratsiri: Data analysis, Conclusion, Recommendation, Writing-reviewing & editing. Ketsarin Chantarasunthon: Data analysis, Conclusion, Recommendation, Writing-reviewing & editing. Wanutsanun Sudsai: Investigation. Pichet Sukprasert: Investigation. Laksamee Chaicharoenwimolkul Chuaitammakit: Conceptualization, Methodology, Validation, Formal analysis, Investigation, Writing-original draft, Visualization, Supervision. Wissawat Sakulsaknimitr: Conceptualization, Methodology, Investigation, Writingoriginal draft, Supervision, Project administration.

Conflict of interest

The authors declare that they have no known competing financial interests or personal relationships that could have appeared to influence the work reported in this paper.

References

1. Leslie HA, van Velzen MJM, Brandsma SH, et al. (2021) Discovery and quantification of plastic pollution in human blood. Environ Int 163: 107199. https://doi.org/10.1016/j.envint.2022.107199

2. Raheem AB, Noor ZZ, Hassan A, et al. (2019) Current developments in chemical recycling of post-consumer polyethylene terephthalate wastes for new materials production: A review. J Clean Prod. 225: 1052–1064. https://doi.org/10.1016/j.jclepro.2019.04.019

3. Benyathiar P, Kumar P, Carpenter G, et at. (2022) Polyethylene Terephthalate (PET) Bottle-toBottle Recycling for the Beverage Industry: A Review. Polymers 14: 2366.

https://doi.org/10.3390/polym14122366

4. Zhang Q, Huang R, Yao H, et al. (2021) Removal of Zn2+from polyethylene terephthalate (PET) glycolytic monomers by sulfonic acid cation exchange resin. J Environ Chem Eng 9:105326. https://doi.org/10.1016/j.jece.2021.105326

5. Vieira CO, Grice JE, Roberts MS, et al. (2018) ZnO:SBA-15 nanocomposites for potential use in sunscreen: Preparation, properties, human skin penetration and toxicity. Skin Pharmacol Physiol 32: 32–42. https://doi.org/10.1159/000491758

6. Imran M, Kim DH, Al-Masry WA, et al. (2013) Manganese-, cobalt-, and zinc-based mixedoxide spinels as novel catalysts for the chemical recycling of poly(ethylene terephthalate) via glycolysis. Polym Degrad https://doi.org/10.1016/j.polymdegradstab.2013.01.007 Stab. 98: 904–915.

7. Kawkumpa S, Saisema T, Seoob O, et al. (2019) Synthesis of polyurethane from glycolysis product of PET using ZnO as catalyst. RMUTSB Acad J 7: 29–39 https://li01.tcithaijo.org/index.php/rmutsb-sci/article/view/150479

8. Shen Z, Zhou H, Chen H, et al. (2018) Synthesis of Nano-Zinc Oxide Loaded on Mesoporous Silica by Coordination Effect and Its Photocatalytic Degradation Property of Methyl Orange. Nanomater 8: 317. https://doi.org/10.3390/nano8050317

9. Nguyen QNK, Yen NT, Hau ND, et al. (2020) Synthesis and Characterization of Mesoporous Silica SBA-15 and ZnO/SBA-15 Photocatalytic Materials from the Ash of Brickyards. J Chem Article ID 8456194, 8 pages: https://doi.org/10.1155/2020/8456194

10. Wen H, Zhou X, Shen Z, et al. (2019) Synthesis of ZnO nanoparticles supported on mesoporous SBA-15 with coordination effect -assist for anti-bacterial assessment. Colloids Surf. B 181: 285294. https://doi.org/10.1016/j.colsurfb.2019.05.055

11. Bhuyan D, Saikia M, Saikia L. (2018) ZnO nanoparticles embedded in SBA-15 as an efficient heterogeneous catalyst for the synthesis of dihydropyrimidinones via Biginelli condensation reaction. Microporous Mesoporous https://doi.org/10.1016/j.micromeso.2017.06.052 Mater 256: 39–48.

12. Pal N, Paul M, Bhaumik A. (2011) Highly ordered Zn-doped mesoporous silica: An efficient catalyst for transesterification reaction. J Solid State Chem 184: 1805–1812. https://doi.org/10.1016/j.jssc.2011.05.033

13. Nagvenkar A, Naik S, Fernandes J. (2015) Zinc oxide as a solid acid catalyst for esterification reaction. Catal Commun 65: 20–23. https://doi.org/10.1016/j.catcom.2015.02.009

14. Yao H, Liu L, Yan D, et al. (2022) Colorless BHET obtained from PET by modified mesoporous catalyst ZnO/SBA-15. https://doi.org/10.1016/j.ces.2021.117109 Chem Eng Sci 248: 117109.

15. Datta B, Pasha MA. (2013) Silica-ZnCl2: An Efficient Catalyst for the Synthesis of 4Methylcoumarins. ISRN Org Chem 13: 1–5. https://doi.org/10.1155/2013/132794

16. Lin CC, Li YY. (2009) Synthesis of ZnO nanowires by thermal decomposition of zinc acetate dihydrate. Mater Chem Phys 113: 334–337. https://doi.org/10.1016/j.matchemphys.2008.07.070

17. Jones F, Tran H, Lindberg D, et al. (2013) Thermal Stability of Zinc Compounds. Energy and Fuels 27: 5663–5669. https://doi.org/10.1021/ef400505u

18. Moosavi A, Sarrafi M, Aghaei A, et al. (2012) Synthesis of mesoporous ZnO/SBA-15 composite via sonochemical route. Micro Nano Lett 7: 130–133. DOI:10.1049/mnl.2011.0461

19. Saha J, Podder J. (2011) Crystallization Of Zinc Sulphate Single Crystals And Its Structural, Thermal And Optical Characterization. J Bangladesh Acad Sci 35: 203–210. https://doi.org/10.3329/jbas.v35i2.9426

20. Foad Raji MP. (2013) Study of Hg(II) species removal from aqueous solution using hybrid ZnCl2-MCM-41 adsorbent. Appl https://doi.org/10.1016/j.apsusc.2013.05.145 Surf Sci 282: 415–424.

21. Jiang Q, Wu ZY, Wang YM, et al. (2006) Fabrication of photoluminescent ZnO/SBA-15 through *directly dispersing zinc nitrate into the as-prepared mesoporous silica occluded with template. J Mater Chem 16: 1536–1542. https://doi.org/10.1039/B516061H*

22. Tay YY, Li S, Sun CQ, et al. (2006) Size dependence of Zn 2p 32 binding energy in nanocrystalline ZnO. Appl Phys Lett 88: 173118. https://doi.org/10.1063/1.2198821

23. Winiarski J, Tylus W, Winiarska K, et al. (2018) XPS and FT-IR Characterization of Selected Synthetic Corrosion Products of Zinc Expected in Neutral Environment Containing Chloride Ions. J Spectrosc Article ID 2079278. https://doi.org/10.1155/2018/2079278

24. Miyao T, Kitai M, Ogita T, et al. (2002) Generation of new acidic sites by dispersing zinc oxide fine particles on silica. Zeitschrift https://doi.org/10.1524/zpch.2002.216.7.931 fur Phys Chemie 216: 931–939.

25. Gabrienko AA, Arzumanov SS, Toktarev AV, et al. (2017) Different Efficiency of Zn2+ and ZnO Species for Methane Activation on Zn-Modified Zeolite. ACS Catal 7: 1818–1830. https://doi.org/10.1021/acscatal.6b03036

26. Zhiyong Y, Bensimon M, Sarria V, et al. (2007) ZnSO4-TiO2 doped catalyst with higher activity in photocatalytic processes. Appl https://doi.org/10.1016/j.apcatb.2007.05.025 Catal B Environ 76: 185–195.

27. Cychosz KA, Thommes M. (2018) Progress in the Physisorption Characterization of Nanoporous Gas Storage https://doi.org/10.1016/j.eng.2018.06.001 Materials. Engineering. 4: 559–566.

28. Lao-Ubol S, Khunlad R, Larpkiattaworn S, et al. (2016) Preparation, Characterization and Catalytic Performance of ZnO-SBA-15 Catalysts. Key Eng Mater 690: 212–217. https://doi.org/10.4028/www.scientific.net/KEM.690.212

Conversion of chromium from simulated batik waste through the utilization of gamma irradiation technique to produce potassium dichromate

Sugili Putra*, Fifi Nurfiana, Junita Sari and Waringin M. Yusmaman
Polytechnic Institute of Nuclear Technology, National Research and Innovation Agency, Jl. Babarsari Kotak POB 6101/YKKB, Yogyakarta 55281, Indonesia

ABSTRACT

Chromium (Cr(VI)) is a type of hazardous waste generated by the batik industry. In this study, the gamma irradiation technique was applied to precipitate chromium in simulated batik mordanting waste. Gamma irradiation induced the generation of active species, including hydrated electrons (eaq-) and hydrogen atoms (•H), which effectively reduced Cr(VI) ions to Cr(III) and caused precipitation as chromium hydroxide (Cr(OH)3) upon interaction with hydroxide ions (OH-). Optimal precipitation conditions were observed at 40 kGy irradiation dose, 4M of 2-propanol work as scavenger, and pH 9. The applied reaction conditions led to a decrease in the concentration of Cr(VI) in simulated waste from 11,673 ppm to 177 ppm. The Cr(OH)3 was calcined to form chromium oxide (Cr2O3) and through a chemical process was synthesized back into K2Cr2O7 with the total Cr recovery of 63.39%. SEM and FTIR analysis indicated that the recovery of Cr(VI) into Cr(OH)3, Cr2O3, and K2Cr2O7 can be considered successful.

Keywords: potassium dichromate; batik waste; gamma irradiation; chromium

1. Introduction

Batik has developed and evolved throughout its extensive journey. Originating from the limited environment of the palace, batik has now evolved into one of Indonesia's creative industry commodities entering the global market. Batik is a motif technique that uses "canting" or stamps as its drawing media, and the colors of batik itself are applied using dyes. There are two types of dye materials for batik: Natural dyes are extracted from natural substances and synthetic dyes, which are artificial dyes produced by factories [1]. Batik was officially recognized by UNESCO as a Masterpiece of the Oral and Intangible Heritage of Humanity on October 2, 2009 [2]. The formal recognition from international institutions regarding batik can be assumed to have a positive correlation with the increased production and consumer demand for batik. The batik industry has long been a sector that significantly contributes to the national economy.

In addition to the positive impacts it has brought, the development of the batik industry has also raised environmental issues due to the potential pollution from its waste. The waste, characterized by dark color and containing hazardous heavy metals, is generated during the batik process, which includes mordanting, waxing, dyeing, fixation, and the final stripping process [3]. Besides that, toxic heavy metal compounds found in the industrial waste of batik include chromium (Cr), lead (Pb), nickel (Ni), copper (Cu), and manganese (Mn) [4].

Chromium (Cr(VI)) was come from a process called mordanting. Mordanting was a process to overcome the limitation of natural dyes that were difficult to penetrate into the fabric and prone to fading. Mordanting is employed during dyeing, involving the use of mordant compounds to enhance the dye's affinity for the material/fabric [5]. Some effective and commonly used mordants include potassium aluminum sulfate (KAl(SO4)2); potassium dichromate (K2Cr2O7); iron(II) sulfate (FeSO4); copper(II) sulfate (CuSO4); and tin(II) chloride (SnCl2) [6].

Cr(VI) heavy metal is a persistent, highly bioaccumulative, and toxic chemical that does not easily degrade in the environment and accumulates in the body through the food chain[7]. The toxicity of chromium species depends significantly on its oxidation state. Chromium as Cr(VI) is toxic and considered carcinogenic, while chromium as Cr(III) is an essential micronutrient for humans[7]. The waste of Cr(VI) heavy metal is one of the hazardous wastes in the batik industry.

The heavy metal Cr(VI) in the liquid waste must be treated to become less hazardous before being safely disposed into the environment to reduce its toxicity by reducing it to Cr(III). Recent advancements in removal technique of Cr(VI) toxic ion from aqueous solution are adsorption, membrane technology, photocatalyst, electrochemical treatment, microbial treatment, microbial fuel cell, floatation, and ion exchange [8]. However, dealing with these methods has a fundamental disadvantage, namely the occurrence of secondary contamination in waste and the need for the use of reagents to separate deposits. Therefore, a new approach is needed to overcome these drawbacks, including utilizing the gamma irradiation technique.

When gamma rays hit a medium in the form of a solution, radiolysis reactions occur, producing radical species such as hydrated electrons (eaq-), hydrogen atoms (•H), and hydroxyl radicals (•OH) [9–11]. The bracketed values with reactive species produced from radiolysis of water depicts radiation chemical yield (G-value), the number of species (i.e., atoms, ions, and molecules) in micromole (μmol) formed or consumed by 1 J of absorbed radiation energy[12]. The strong reducing effect of hydrated electrons (eaq-) and hydrogen atoms (•H) can directly reduce Cr(VI) ions to a lower valence state, turning them into Cr(III) that forms precipitate when reacting with hydroxide ions (OH-) present in wastewater as shown in the Eqs 1–4[13]. This reaction forms a Cr(OH)3 precipitate, which can be separated by ordinary filtration.

$$H_2O \rightarrow e_{aq}^{-}\ (0.28), \bullet H(0.06), \bullet OH(0.29), H_2(0.047), H_2O_2(0.07), H_3O^{+}(0.27) \tag{1}$$

$$Cr^{6+} + 3\, e_{aq}^{-} \rightarrow Cr^{3+} \tag{2}$$

$$Cr^{6+} + 3 \bullet H \rightarrow Cr^{3+} + 3H^{+} \tag{3}$$

$$Cr^{3+} + 3OH^{-} \rightarrow Cr(OH)_3 \downarrow \tag{4}$$

The presence of hydroxyl radicals (•OH), which act as oxidizers, can interfere with the precipitation process, but their presence can be eliminated using a scavenger. Scavengers that can be used include 2-propanol, t-butanol, formic acid, and sodium formate [10,13]. The scavenger used in this study is 2-propanol.

The precipitation process of Cr with the radiolytic reduction method will be optimal in the pH range of 7–9.5. At a pH that is too low, hydrated electrons are quickly captured by hydrogen ions and converted into hydrogen atoms. On the other hand, at a pH above 9.5, it causes G-values for •OH and eaq- decrease [10]. Additionally, Cr(III) compound will remain soluble at low pH and will begin to precipitate as Cr(OH)3, reaching a maximum at pH 7 to 9.72 [14]. If Cr(OH)3 is heated, Cr2O3 will be formed [9,13].

The difference between this research and the other research involving the reduction of Cr(VI) to Cr(III) is the uniqueness of batik waste composition. The batik waste contains dyes and wax that may influence the reduction and precipitation processes of chromium. In this research, the effect of irradiation doses, pH, and scavenger concentrations was studied to determine the optimal conditions for the formation of Cr precipitates from simulated liquid waste of batik using gamma irradiation.

Furthermore, the formed Cr precipitates will be converted back into potassium dichromate through a chemical process so that the potassium dichromate can be reused. The percentage recovery of the resulting potassium dichromate from this recycling process was calculated.

2. Materials and methods

2.1. Materials

Jalawe fruit skin, batik wax, potassium dichromate (K2Cr2O7) from Merck, pro analysis 2propanol from Merck, perchloric acid (HClO4) from Supelco, sodium hydroxide (NaOH) from Merck, and aquadest from Merck Millipore with resistance 18.2 MOhm.cm were used in this study.

2.2. Instrumentation

A type I of gamma irradiator with a Co-60 radioactive source was used to irradiated sample. The irradiator was installed at Polytechnic Institute of Nuclear Technology BRIN with dose rate 2.930 kGy/h at November, 2022. The irradiator has been calibrated with reference from Riso High Dose Reference Laboratory, Technical University of Denmark. B3 DoseStix was used as dosimeter. Monitoring the pH solution was used a pH/C meter Hanna Instruments HI 2210, remained Cr(VI) concentration in sample solution was determined used XRF Rigaku Nex QC by generated standar curve of Cr(VI) from K2Cr2O7. Analysis of solid samples resulted from precipitation was done with FTIR Shimadzu IR-Spirit and SEM-EDS Hitachi Su3500.

2.3. Procedures

2.3.1. Prepared simulated liquid batik mordanting waste (receipt from batik craftsmen in Giriloyo, Yogyakarta, Indonesia)

The 50 grams of Jalawe fruit skin in 500 ml of water was boiled for 2 hours, the filtrate was taken to get the natural dyes. The 3.3 grams of K2Cr2O7 was added with 1 ml of natural dye from the extract of Jalawe fruit skin that has been made and 0.02 grams batik wax. The mixture was dissolved in 100 ml of water and stirred.

2.3.2. Separation of wax from waste solution

The liquid waste from batik fixation was filtered with Whatman paper to separate wax from the waste solution.

2.3.3. Effect of scavenger concentration on the Cr precipitation

The simulated waste was added with 2-propanol at variations of 1M, 2M, 4M, 6M, 8M, and irradiated at a dose of 40 kGy, as well as measured the pH of the waste. The obtained precipitate was dried in an oven at 105 °C for 2 hours, and the formed precipitate was weighed and the remained Cr(VI) at solution was measured.

2.3.4. Effect of irradiation dose on the Cr precipitation

The simulated waste was added with optimum scavenger concentration and irradiated at dose 10, 20, 30, 40, and 50 kGy and measured the pH of the waste. The obtained precipitate was dried in an oven at

105 °C for 2 hours. The formed precipitate was weighed and the remained Cr(VI) at solution was measured.

2.3.6. Chromium recovery from simulated waste through gamma irradiation

The simulated waste was added with optimum scavenger concentration and conditioned at optimum pH, and Irradiated at optimum irradiation dose. The precipitate was filtered with Whatman paper and dried the precipitate at 105 °C for 2 hours. It was expected that Cr(OH)3 is formed. Weighed the Cr(OH)3 precipitate.

2.3.7. Synthesis of potassium dichromate [14]

The obtained Cr(OH)3 precipitate was calcined at 500 °C for 5 hours. It was expected that Cr2O3 formed in this process. KOH was heated at 200 °C, after KOH melted completely, was added Cr2O3 with a mass ratio of KOH to Cr2O3 is 2:1. KNO3 was added to the mixture with a mass ratio of KNO3 to Cr2O3 is 3:1. The mixture was mixed until homogenous and becomes a thick paste. The mixture was cooled and dissolved at 100 ml of aquadest then heated until dissolved. The solution was filtered and the obtained filtrate was collected in an evaporating dish (a yellow filtrate).

The filtrate was heated at 120 °C until saturated, added glacial acetic acid dropwise while stirred (until it turned orange-red and did not change anymore). The filtrate was cooled immediately in an ice bath until crystals formed. The formed crystal was filtered then dried at 150 °C and weighed its mass. The percentage of chromium (Cr) recovery was calculated.

3. Results and discussion

3.1. Effect of scavenger concentration on the Cr precipitation

A scavenger is a radical attractor intentionally added to control the products of a reaction. In the context of the deposition of Cr(VI) into Cr(III) in the form Cr(OH)3, the scavenger will attract •OH radicals thereby preventing the re-oxidation of Cr(III) back into Cr(VI) by reacting with •OH radicals.

In this study, 2-propanol was employed as the scavenger. The 2-propanol reacts with •OH radicals (oxidative) and form reducing (CH3)2C•OH radicals according to the reaction (6). Therefore, when adding a scavenger, the number of reducing radicals (G-value) in solution could be increased twice. Both solvated electrons and (CH3)2C•OH radicals participate in reduction of Cr(VI) to Cr(III). The contribution of hydrogen radicals to this process is negligible, since their G-value is small. The 2-propanol scavenger was varied with concentrations of 0 M, 1 M, 2 M, 4 M, 6 M, and 8 M. The measured pH of the waste solution before irradiation was 4.3 and the waste was irradiated 40.0 kGy. The graph showed that the lowest mass of Cr(OH)3 precipitate was reached without the addition of 2-propanol scavenger. This occurs due to the absence of the radical scavenger, so that the hydroxyl ions (•OH) reacting with reduced Cr(III) ions. As a result, Cr(III) ions oxidize back to Cr(VI) ions without reacting with hydroxide ions (OH-) as shown at Eq 5.

$$Cr^{3+} + 3\mathrm{OH}\bullet \rightarrow Cr^{6+} + 3OH^{-} \tag{5}$$

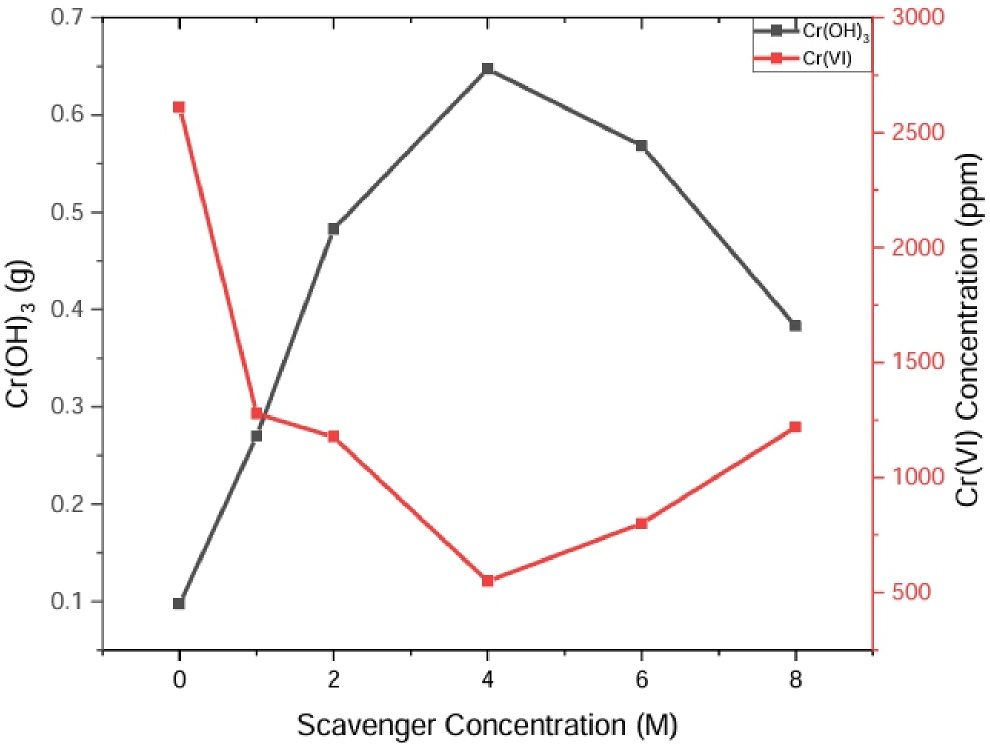

Figure 1. The mass of the formed Cr(OH)3 precipitate and the remaining concentration Cr(VI) in the solution as function of scavenger concentration.

The mass of the Cr(OH)3 precipitate increases with the rising concentration of 2-propanol scavenger. The maximum amount of precipitate was observed at a concentration of 4 M followed by decreased Cr(VI) concentration in the solutions. At 6 M and beyond concentration of 2-propanol, the mass of Cr(OH)3 is decreased. This indicates that the optimal capture of hydroxyl radicals (•OH) and hydrogen ions (•H) by 2-propanol occurs at a concentration of 4 M.

$$(CH_3)_2CHOH + \mathrm{OH}\bullet \rightarrow (CH_3)_2C\bullet\mathrm{OH} + H_2O \tag{6}$$

$$(CH_3)_2CHOH + \mathrm{H}\bullet \rightarrow (CH_3)_2C\bullet\mathrm{OH} + H_2 \tag{7}$$

Reactions (6-7) [15] result in the release of one hydrogen atom from 2-propanol, produced the unstable radical (CH3)2C•OH. To achieve stability, this radical reacted with Cr(VI) ions to created Cr(III) and C3H6O (propanal) as the products (Eq 8). Furthermore, the formed Cr(III) ions reacted with hydroxide ions (OH-) to form the Cr(OH)3 precipitate.

$$[3(CH_3)_2C\bullet\mathrm{OH} + Cr^{6+} \rightarrow Cr^{3+} + 3H^+ + 3C_3H_6O \tag{8}$$

Increasing the concentration of 2-propanol after 6 M will decrease the mass of Cr(OH)3 precipitate. This occurs because the excessive concentration of 2-propanol scavenger competes with hexavalent chromium to react with hydrated electrons (eaq-). According to the calculation, the amount of scavenger needed capture the •OH and •H radicals are 0.14 M, with estimation of precipitated Cr(OH)3 was 0.47 g.

3.2. Effect of irradiation dose on the Cr precipitation

The simulated chromium waste was irradiated with varying doses of 10 kGy, 20 kGy, 30 kGy, 40 kGy, and 50 kGy, with the addition of 4 M 2-propanol as scavenger and the measured pH before irradiation was 4.3. Figure 2 showed that with increasing irradiation doses, the mass of the formed Cr(OH)3 precipitate increased. The optimum mass of the Cr(OH)3 precipitate was observed at dose 40 kGy, but followed by a decreased at dose 50 kGy.

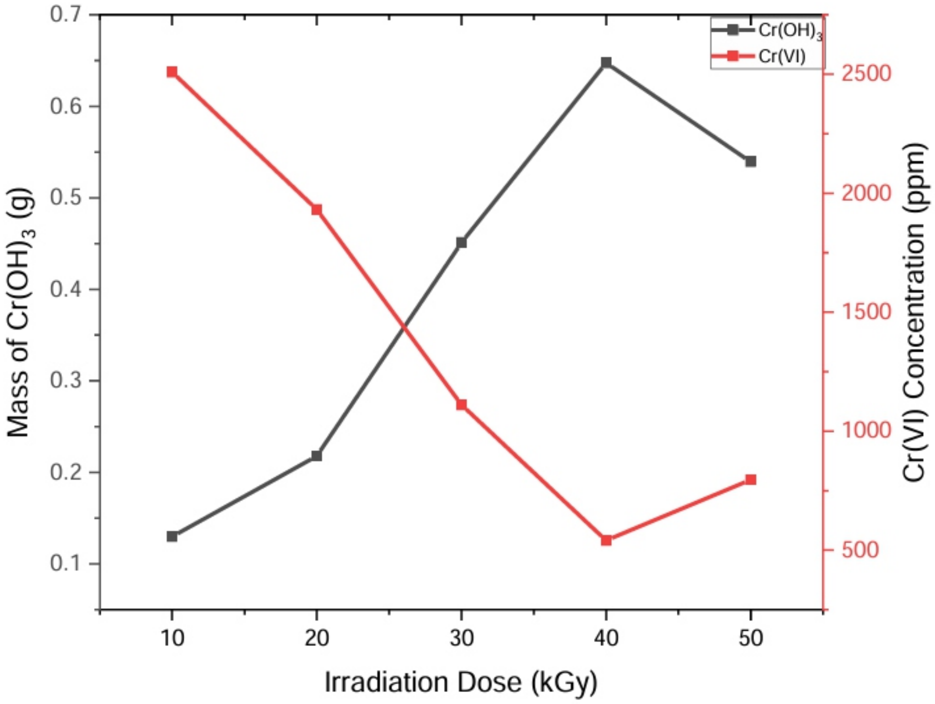

Figure 2. The mass of the formed Cr(OH)3 precipitate and the remaining Cr(VI) concentration in the solution as function of total irradiation dose.

The increase in the mass of the Cr(OH)3 precipitate occurs because the amount of reducing agents produced is influenced by the absorbed dose. The higher the irradiation dose, the more reducing agents were generated from the radiolysis process. These agents reduced Cr(VI) ions to lower-charged chromium ions (Cr(III)). As a result, the concentration of Cr(VI) in the waste decreased and the formed Cr(OH)3 precipitate increased.

At a dose 50 kGy, there is a decreased in the mass of the formed Cr(OH)3 precipitate or an increase in the remaining Cr(VI) in the solution. This is due to the larger radiation intensity applied to the sample, causing more hydroxyl radical (•OH) compounds to be generated in the solution through water radiolysis. Consequently, the concentration of 2-propanol scavenger used should be higher. The concentration of the scavenger used is not sufficient to capture the abundant hydroxyl radicals formed at doses above 40 kGy. As a result, hydroxyl radicals (•OH) react with Cr(III) ions, and the Cr(III) ions are re-oxidized, producing Cr(VI) ions. This leads to an increased in the concentration of Cr(VI) in the waste solution, and the formed Cr(OH)3 precipitate decreased.

3.3. Effect of pH solution on the Cr precipitation

The acidity levels of simulated chromium waste were varied to pH 2, 4, 7, 8, 9, 10, and 11 by adding sulfuric acid (H2SO4) or NaOH. The 4 M of 2-propanol as a scavenger was added, followed by irradiation at a dose of 40 kGy. Figure 3 showed the optimum formation of Cr(OH)3 precipitate and the lowest remains of Cr(VI) was observed at alkaline pH, with the optimum pH was 9. Some studies have reported that the optimum pH for this conditions is between 8.5–9.5 due to the solubility of chromium hydroxide in that range [16,17]. It is rational to expect that the generated Cr(III) could be spontaneously precipitated under alkaline conditions due to the low solubility of Cr(OH)3 (pKsp = 30.2) [17]. However, it dissolves more readily in low or acidic pH conditions. Cr(OH)3 is amphoterous, that can react with both hydrogen and hydroxide ions.

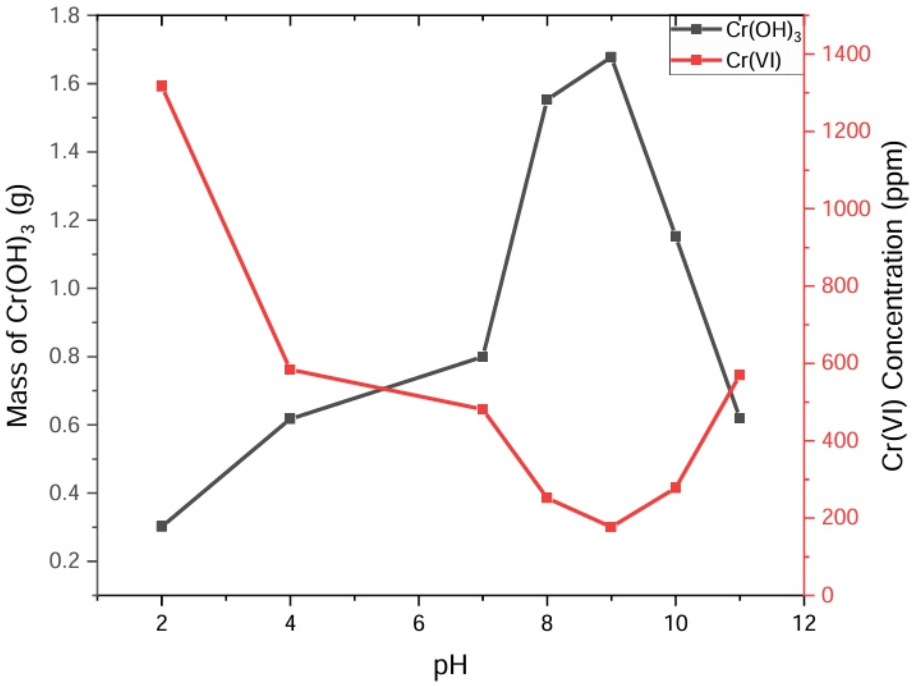

Figure 3. The mass of the formed Cr(OH)3 precipitate and the remaining Cr(VI) concentration in the solution as function of pH.

At pH 2 and 4, which are acidic conditions, an excess of hydrogen ions (H+) was formed, leading to more reactions between hydrogen and hydroxide ions than the precipitation reaction. At pH 8 and the optimal pH of 9, which are alkaline conditions, the formation of an excess of hydrogen ions (H+) was minimized. This ensures that the precipitation reaction was not disturbed by the reaction between hydrogen and hydroxide ions, facilitating the desired Cr(OH)3 precipitation. At pH 7 (neutral conditions), the concentration of hydrogen ions (H+) and hydroxide ions (OH-) was balanced, resulting in no excessive reaction between H+ and OH-, as observed in acidic and alkaline environments. In this condition, Cr(OH)3 precipitation can occur but not optimal. At pH 11 (highly alkaline conditions), if there is an excess of OH-, the Cr(OH)3 precipitate will redissolve, forming tetrahydroxo chromate (III) ions with the following reaction equation:

$$Cr(OH)_3 + OH^- \rightleftharpoons [Cr(OH)_4]^- \tag{9}$$

3.4. Chromium recovery from simulated wastewater treated with gamma irradiation

The optimum conditions for chromium precipitation from the simulated batik fixation waste were at scavenger concentration of 4 M, irradiation dose of 40 kGy, and at alkaline environment with a pH before irradiation was 9. The resulting Cr(OH)3 precipitate under these conditions was 1.678 grams from 3.3 grams of K2Cr2O7 in the simulated waste. The Chromium recovery in this process was 72,6

Chromium(III) Oxide (Cr2O3) formation occurs through the calcined of chromium(III) hydroxide Cr(OH)3 at a temperature of 500 °C for 5 hours as shown at Eq10. From 1.678 grams of Cr(OH)3 was obtained 1.2 grams of Cr2O3. The Chromium recovery in this process was 96.9 %

$$2Cr(OH)_3 \rightarrow Cr_2O_3 + 3H_2O \tag{10}$$

By Heating a mixture of KOH, KNO3, and Cr2O3 was produced a yellow filtrate, namely potassium chromate (K2CrO4). The reaction formed at Eq 11 [18].

$$Cr_2O_3 + 3KNO_3 + 4\,KOH \rightarrow 2K_2Cr_2O_4 + 3KNO_2 + 2H_2O \tag{11}$$

The acidification process was carried out by adding glacial acetic acid to convert potassium chromate into orange-colored potassium dichromate (K2Cr2O7). Potassium dichromate was stable in an acidic environment and the ion's reaction was reversible. In a neutral or alkaline solution, chromate ions are stable, while in an acidic environment, chromate ions are present. Besides accelerating the formation of potassium dichromate, the addition of acetic acid aims to bind impurities that may be present in the potassium dichromate formation process. The reaction that occurs was shown at Eq 12 [18].

$$2K_2CrO_4 + 2CH_3COOH \rightleftharpoons K_2Cr_2O_7 + 2CH_3COOK + H_2O \tag{12}$$

Subsequently, the purification of the resulting potassium dichromate product is carried out using the recrystallization principle, where the substance is cooled directly in an ice bath while in a hot state. This accelerates crystal formation. The next steps involve filtration and drying of the crystals. The mass of potassium dichromate (K2Cr2O7) formed in this process was 2.01 grams from 1.2 grams of Cr2O3. The Chromium recovery in this process was 89.28 %, with the total Cr recovery was 63.39%.

3.5. SEM characterizations of Cr(OH)3, Cr2O3, and K2Cr2O7 obtained from simulated wastewater recovery

The SEM results of Cr(OH)3 (Figure 4a) showed a rough surface at a magnification of 2000 times. This aligned with previous study which states that at the micrometer scale Cr(OH)3 SEM results showed a rougher surface compared to Cr2O3 [19]. The C2O3 (Figure 4b) particles appear smaller than Cr(OH)3 and showed concave pits indicating water loss in the Cr2O3 formation through calcination. SEM results for Cr2O3 showed that all particles exhibit a spherical shape with a high level of agglomeration among fine particles. Potassium dichromate crystals (Figure 4c) appear as fine particles or particle clusters.

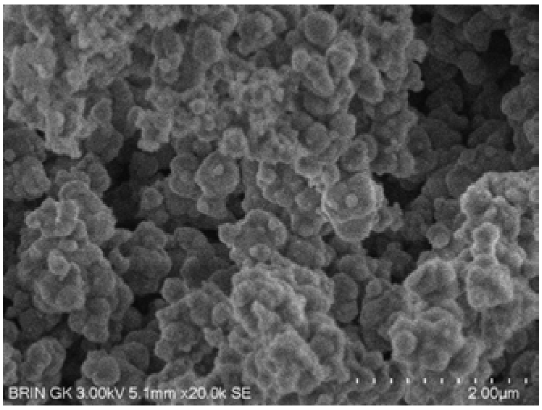

(a)

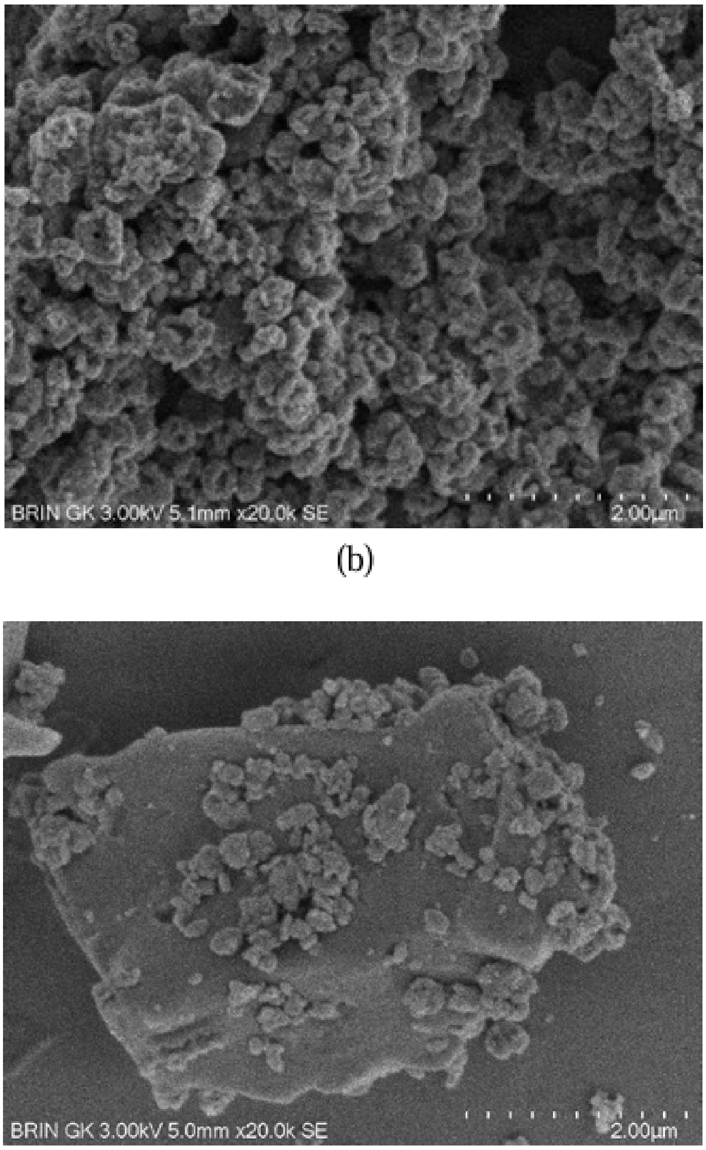

(b)

(c)

Figure 4 [illegible] K2Cr2O7.

3.6. FTIR characterizations of Cr(OH)3, Cr2O3, and K2Cr2O7 obtained from simulated wastewater recovery

Figure 5 (a) showed the FTIR spectrum of the Cr(OH)3 precipitate sample. An absorption band at around 940 cm-1 was assigned to stretching vibrations of the Cr-O bond [20]. The two weak and broad bands at about 1630 cm-1 and 3400 cm-1 are due to the O-H vibration of water molecules adsorbed on the surfaces [21]. The peaks at 1480 cm-1 and 1370 cm-1 can be assigned to the splitting of the asymmetric stretching of metal carbonate [22] absorbed from the air during the synthesis. Figure 5(b) presented the FTIR spectrum of the Cr2O3 sample calcined at 500 °C. The result aligned with previous research which showed two sharp peaks at 575 and 630 cm-1 assigned to the Cr

O stretching [21]. The peak at 3416 cm-1 is attributed to the stretching of O-H from hydroxyl groups bonded with H. Peaks at 1039 cm-1 and 1628 cm-1 represent the bending vibration of H-O-H from physically adsorbed water molecules. The peak at 950 cm-1 is associated with the stretching of Cr-O bonds.

Figure 5 (c) presented the FTIR spectrum of the K2Cr2O7 sample and commercial one. The result showed peak at 555 and 754 cm-1 confirming the previous studies. The peak at the wavenumber of 555 cm-1 was caused by the symmetric stretching vibration of Cr-O-Cr, while the peak at 754 cm-1 was caused by the anti-symmetric stretching vibration of Cr-O-Cr [23]. The peak at the wavenumber of 891 cm-1 was attributed to the symmetric stretching vibration of Cr-O3, while the very intense peak at 935 cm-1 was caused by the asymmetric stretching vibration of Cr-O3 [23]. It can be observed that there was no significant difference between the peaks of the K2Cr2O7 sample and the K2Cr2O7 commercial product. This indicated that the recovery of Cr(VI) into K2Cr2O7 can be considered successful.

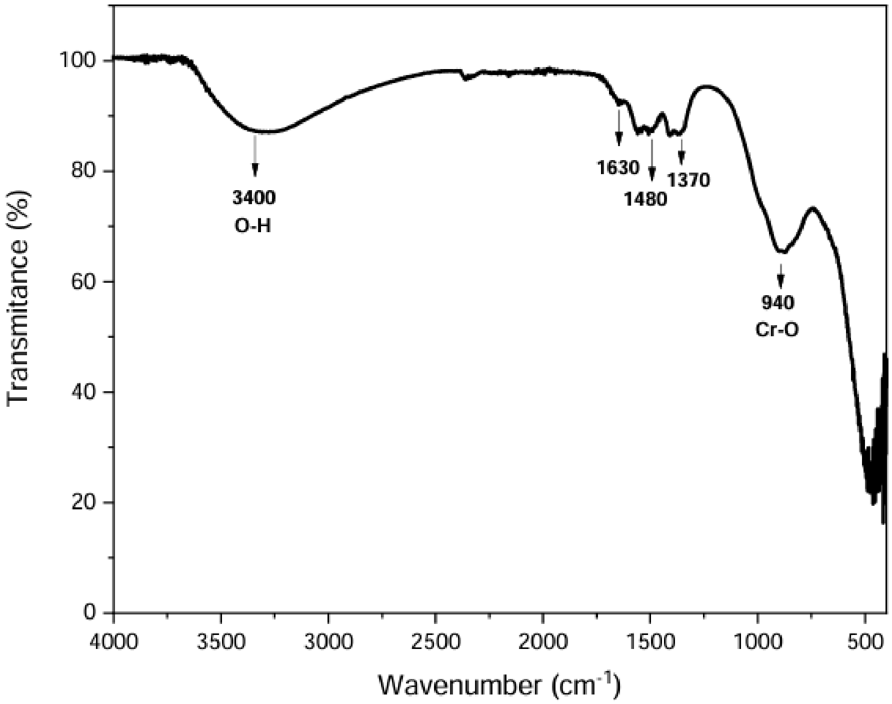

(a)

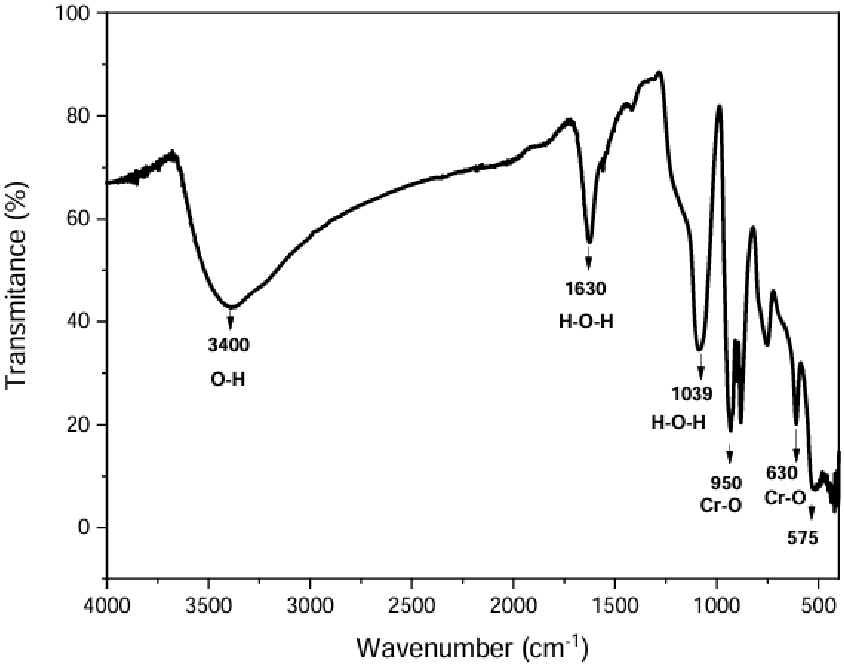

(b)

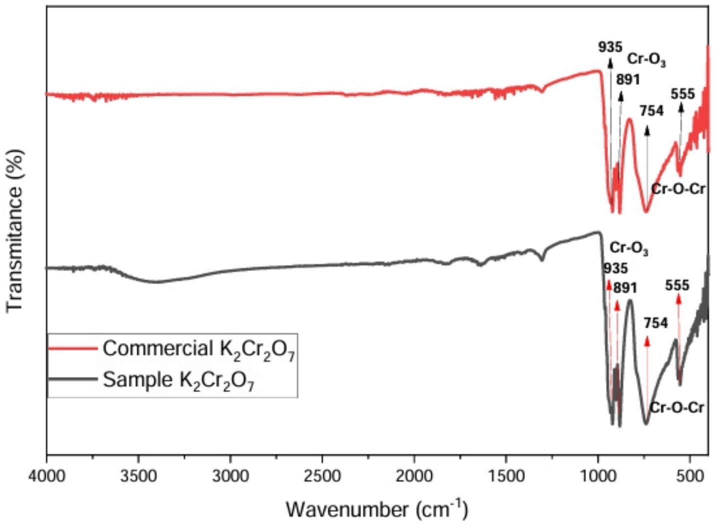

(c)

Figure 5. FTIR spectrum of (a) Cr(OH)3, (b) Cr2O3, and (c) K2Cr2O7 sample and commercial

4. Conclusions

The reduction of Cr(VI) to Cr(III) was carried in the synthetic chrome mordanting batik waste by gamma radiolysis of water in the presence of natural jalawe dye and the wax. Optimal conditions were observed at 40 kGy irradiation dose, 4M of 2-propanol work as scavenger, and pH 9. Radiolytic precipitation produced Cr(OH)3, followed by calcination to form Cr2O3. Through a chemical process, Cr2O3 can be change back to K2Cr2O7. The SEM and FTIR result revealed that the recovery of Cr(VI) into Cr(OH)3, Cr2O3, and K2Cr2O7 can be considered successful.

Use of AI tools declaration

The authors declare they have not used Artificial Intelligence (AI) tools in the creation of this article.

Acknowledgments The authors gratefully acknowledge financial and infrastructure support from the Polytechnic Institute of Nuclear Technology, National Research and Innovation Agency of Indonesia.

Conflict of interest

The authors declare that they have no personal interest that could have appeared to influence the work reported in this paper.

References

1. Purwanto P (2019) Exploration of natural dyes as alternative substitutes of synthetic dyes on batik making fabrics. J Phys Conf Ser 1375: 12–23. https://doi:10.1088/1742-6596/1375/1/012023.

2. Pramugani A, Soda S, Argo T A (2020) Current situation of batik wastewater treatment in Pekalongan City, Indonesia. Civ Eng 8: 188–193. J Japan Soc https://doi.org/10.2208/journalofjsce.8.1_188.

3. Alamsyah A, Maziyah S, Supriyono A (2020) Natural Coloring as a Coloring Material for Batik Craft in Jepara. Proceedings of the 4th International Conference on Indonesian Social and Political Enquiries, ICISPE 2019, 21–22 October 2019, Semarang, Central Java, Indonesia. http://dx.doi.org/10.4108/eai.21-10-2019.2294350.

4. Natalina N, Firdaus H (2018) Penurunan Kadar Kromium Heksavalen (Cr6+) Dalam Limbah Batik

Limbah Udang (Kitosan). http://doi:10.14710/teknik.v38n2.13403. Teknik. 38: 99–102.

5. Sarwono Darwoto, Adi S P (2022) Utilizing Indigofera Natural Dyes to Develop Batik. IOP Conf Ser Earth Environ Sci 1114: 12–40. http://doi:10.1088/1755-1315/1114/1/012040. 5th Int

6. Yılmaz F, Bahtiyari M İ (2017) Investigation of the usability of Hibiscus plant as a natural dye source. Symp Innov Technol Eng Sci 952–956. https://isites.info/PastConferences/ISITES2017/ISITES2017/papers/C3-ISITES2017ID179.pdf.

7. Wang Y, Su H, Gu Y, et al. (2017) Carcinogenicity of chromium and chemoprevention: A brief update. Onco Targets Ther 10: 4065–4079. https://doi.org/10.2147/OTT.S139262.

8. Karimi-Maleh H, Ayati A, Ghanbari S, et al. (2021) Recent advances in removal techniques of Cr(VI) toxic ion from aqueous solution: A comprehensive review. J Mol Liq 329: 115062. https://doi.org/10.1016/j.molliq.2020.115062.

9. Alrehaily LM, Joseph JM, Musa AY, et al. (2013) Gamma-radiation induced formation of chromium oxide nanoparticles from dissolved dichromate. Phys Chem Chem Phys 15: 98–107. https://doi.org/10.1039/c2cp43150e.

10. Shrivastava KC, Pandey SP, Kumar SA, et al. (2020) Remediation of chromium(VI) ions as chromium oxide xerogel via gamma-radiolysis of aqueous waste discharge. Sep Purif Technol 236: 116291. https://doi.org/10.1016/j.seppur.2019.116291.

11. Djouider F (2012) Radiolytic formation of non-toxic Cr(III) from toxic Cr(VI) in formate containing aqueous solutions: A system for water treatment. J Hazard Mater 223–224: 104–109. http://dx.doi.org/10.1016/j.jhazmat.2012.04.059.

12. Shah NS, Khan J A, Sayed M, et al. (2020) Synergistic effects of H2O2 and S2O82− in the gamma radiation induced degradation of congo-red dye: Kinetics and toxicities evaluation. Sep Purif Technol 233: 115966. https://doi.org/10.1016/j.seppur.2019.115966.

13. Alrehaily LM, Joseph JM, Wren J C (2015) Radiation-induced formation of chromium oxide nanoparticles: Role of radical scavengers on the redox kinetics and particle size. J Phys Chem C 119: 16321–16330. https://doi.org/10.1021/acs.jpcc.5b02540.

14. Rai D, Sass BM, Moore DA (1987) Chromium(III) Hydrolysis Constants and Solubility of Chromium(III) Hydroxide. Inorg Chem 26: 345–349. https://doi.org/10.1021/ic00250a002.

15. Li Z, Yang Y, Relefors A, et al. (2021) Tuning morphology, composition and oxygen reduction reaction (ORR) catalytic performance of manganese oxide particles fabricated by γ-radiation induced synthesis. J Colloid Interface Sci 583: 71–79. https://doi.org/10.1016/j.jcis.2020.09.011.

16. Choppala G, Bolan N, Park J H (2013) Chromium Contamination and Its Risk Management in Complex Environmental Settings. Advances in Agronomy. 120: 129–171. http://dx.doi.org/10.1016/B978-0-12-407686-0.00002-6.

17. Xie B, Shan C, Xu Z, et al. (2017) One-step removal of Cr(VI) at alkaline pH by UV/sulfite process: Reduction to Cr(III) and in situ Cr(III) precipitation. Chem Eng J 308: 791–797. https://doi.org/10.1016/j.cej.2016.09.123.

18. Zhi Sun, Yi Zhang, SL Zheng. (2009) A New Method of Potassium Chromate Production from Chromite and KOH-KNO3-H2O Binary Submolten Salt System. AIChE J 55: 2646–2656. https://doi.org/10.1002/aic.11871

19. Gomes ASO, Simic N, Wildlock M, et al. (2018) Electrochemical Investigation of the Hydrogen Evolution Reaction on Electrodeposited Films of Cr(OH)3 and Cr2O3 in Mild Alkaline Solutions. Electrocatalysis 9: 333–342. https://doi.org/10.1007/s12678-017-0435-1.

20. Mao, L., Gao, B., Deng, N., et al. (2016) Oxidation behavior of Cr(III) during thermal treatment of chromium hydroxide in the presence of alkali and alkaline earth metal chlorides. Chemosphere 145: 1–9. http://dx.doi.org/10.1016/j.chemosphere.2015.11.053.

21. Khalaji AD (2020) Cr2O3 Nanoparticles: Synthesis, Characterization, and Magnetic Properties. Nanochemistry Res 5: 148–153. https://doi.org/10.22036/ncr.2020.02.005

22. Makhloufi S, Omari E, Omari M (2019) Synthesis, characterization, and electrocatalytic properties of La0.9Sr0.1Cr1−xCo xO3 perovskite oxides. J Aust Ceram Soc 55: 1–10. https://doi.org/10.1007/s41779-018-0204-5.

23. Azeez HS, Mohammad M R (2017) Study the Structure, Morphology and Vibration Modes for K2CrO4 and K2Cr2O7. J Al-Nahrain Univ 20: 71–76. https://doi.org/10.22401/JUNS.20.2.09.

Instructions for Authors

Essentials for Publishing in this Journal

1 Submitted articles should not have been previously published or be currently under consideration for publication elsewhere.

2 Conference papers may only be submitted if the paper has been completely re-written (taken to mean more than 50%) and the author has cleared any necessary permission with the copyright owner if it has been previously copyrighted.

3 All our articles are refereed through a double-blind process.

4 All authors must declare they have read and agreed to the content of the submitted article and must sign a declaration correspond to the originality of the article.

Submission Process

All articles for this journal must be submitted using our online submissions system. http://enrichedpub.com/ . Please use the Submit Your Article link in the Author Service area.

Manuscript Guidelines

The instructions to authors about the article preparation for publication in the Manuscripts are submitted online, through the e-Ur (Electronic editing) system, developed by **Enriched Publications Pvt. Ltd**. The article should contain the abstract with keywords, introduction, body, conclusion, references and the summary in English language (without heading and subheading enumeration). The article length should not exceed 16 pages of A4 paper format.

Title

The title should be informative. It is in both Journal's and author's best interest to use terms suitable. For indexing and word search. If there are no such terms in the title, the author is strongly advised to add a subtitle. The title should be given in English as well. The titles precede the abstract and the summary in an appropriate language.

Letterhead Title

The letterhead title is given at a top of each page for easier identification of article copies in an Electronic form in particular. It contains the author's surname and first name initial .article title, journal title and collation (year, volume, and issue, first and last page). The journal and article titles can be given in a shortened form.

Author's Name

Full name(s) of author(s) should be used. It is advisable to give the middle initial. Names are given in their original form.

Contact Details

The postal address or the e-mail address of the author (usually of the first one if there are more Authors) is given in the footnote at the bottom of the first page.

Type of Articles

Classification of articles is a duty of the editorial staff and is of special importance. Referees and the members of the editorial staff, or section editors, can propose a category, but the editor-in-chief has the sole responsibility for their classification. Journal articles are classified as follows:

Scientific articles:

1. Original scientific paper (giving the previously unpublished results of the author's own research based on management methods).

2. Survey paper (giving an original, detailed and critical view of a research problem or an area to which the author has made a contribution visible through his self-citation);

3. Short or preliminary communication (original management paper of full format but of a smaller extent or of a preliminary character);

4. Scientific critique or forum (discussion on a particular scientific topic, based exclusively on management argumentation) and commentaries. Exceptionally, in particular areas, a scientific paper in the Journal can be in a form of a monograph or a critical edition of scientific data (historical, archival, lexicographic, bibliographic, data survey, etc.) which were unknown or hardly accessible for scientific research.

Professional articles:

1. Professional paper (contribution offering experience useful for improvement of professional practice but not necessarily based on scientific methods);
2. Informative contribution (editorial, commentary, etc.);
3. Review (of a book, software, case study, scientific event, etc.)

Language

The article should be in English. The grammar and style of the article should be of good quality. The systematized text should be without abbreviations (except standard ones). All measurements must be in SI units. The sequence of formulae is denoted in Arabic numerals in parentheses on the right-hand side.

Abstract and Summary

An abstract is a concise informative presentation of the article content for fast and accurate Evaluation of its relevance. It is both in the Editorial Office's and the author's best interest for an abstract to contain terms often used for indexing and article search. The abstract describes the purpose of the study and the methods, outlines the findings and state the conclusions. A 100- to 250-Word abstract should be placed between the title and the keywords with the body text to follow. Besides an abstract are advised to have a summary in English, at the end of the article, after the Reference list. The summary should be structured and long up to 1/10 of the article length (it is more extensive than the abstract).

Keywords

Keywords are terms or phrases showing adequately the article content for indexing and search purposes. They should be allocated heaving in mind widely accepted international sources (index, dictionary or thesaurus), such as the Web of Science keyword list for science in general. The higher their usage frequency is the better. Up to 10 keywords immediately follow the abstract and the summary, in respective languages.

Acknowledgements

The name and the number of the project or programmed within which the article was realized is given in a separate note at the bottom of the first page together with the name of the institution which financially supported the project or programmed.

Tables and Illustrations

All the captions should be in the original language as well as in English, together with the texts in illustrations if possible. Tables are typed in the same style as the text and are denoted by numerals at the top. Photographs and drawings, placed appropriately in the text, should be clear, precise and suitable for reproduction. Drawings should be created in Word or Corel.

Citation in the Text

Citation in the text must be uniform. When citing references in the text, use the reference number set in square brackets from the Reference list at the end of the article.

Footnotes

Footnotes are given at the bottom of the page with the text they refer to. They can contain less relevant details, additional explanations or used sources (e.g. scientific material, manuals). They cannot replace the cited literature.

The article should be accompanied with a cover letter with the information about the author(s): surname, middle initial, first name, and citizen personal number, rank, title, e-mail address, and affiliation address, home address including municipality, phone number in the office and at home (or a mobile phone number). The cover letter should state the type of the article and tell which illustrations are original and which are not.

Note